DANISH METEOROLOGICAL INSTITUTE

—— SCIENTIFIC REPORT ——

02-15

Probabilistic Analysis of Atmospheric Transport Patterns from Nuclear Risk Sites in Euro-Arctic Region
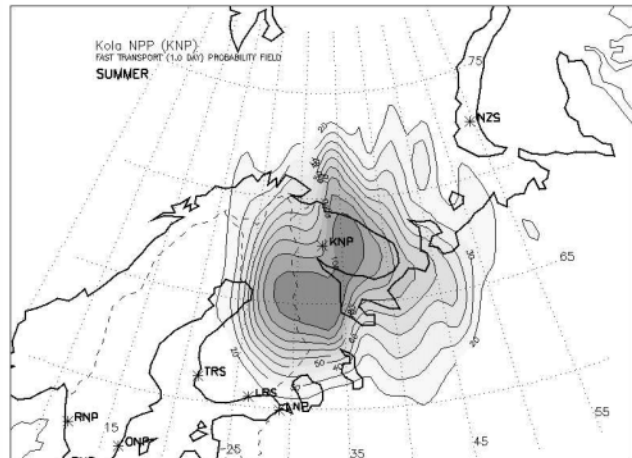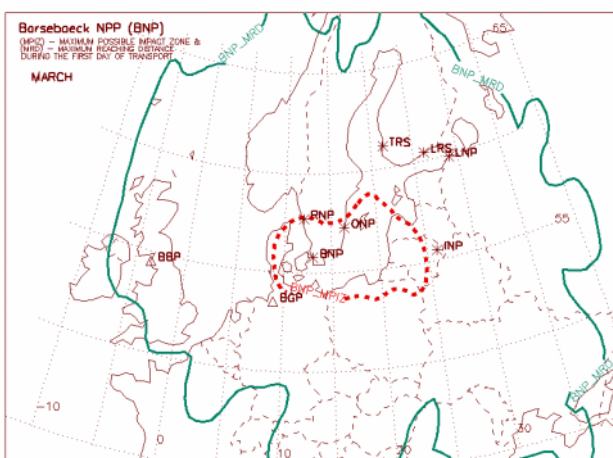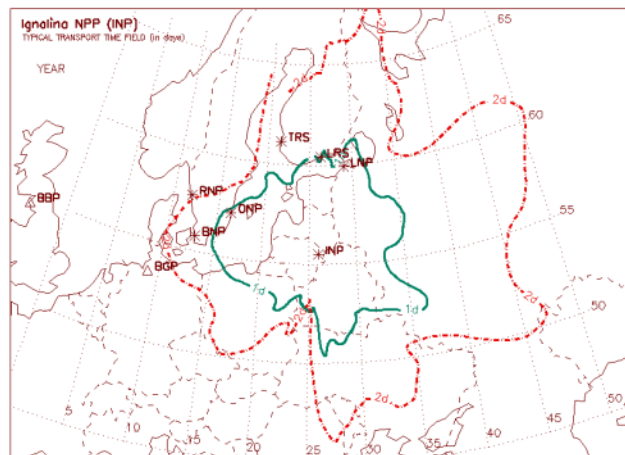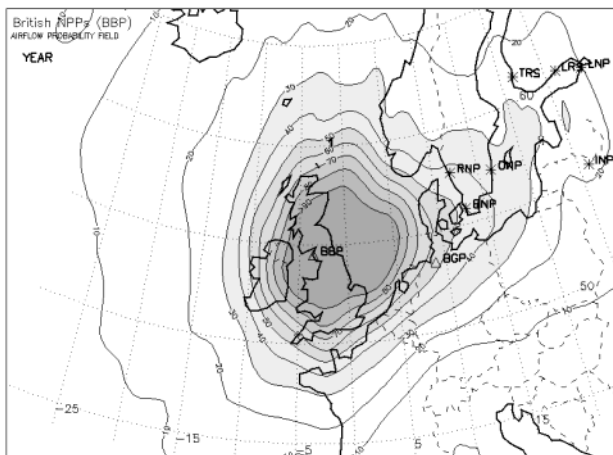
Alexander Mahura[1,2] and Alexander Baklanov[1]

[1] Danish Meteorological Institute, Copenhagen, Denmark
[2] Institute of Northern Environmental Problems, Kola Science Center, Apatity, Russia

'Arctic Risk' Project of the Nordic Arctic Research Programme (NARP)

COPENHAGEN 2002

TABLE OF CONTENTS

SUMMARY

The main aim of this study is 1) to test methodology for evaluation of the possible atmospheric transport of radioactivity from the nuclear risk sites (NRSs) to different geographical regions and countries, and 2) to combine atmospheric transport modeling and statistical analyses to evaluate possible impact of an accidental release from main NRSs located in the Euro-Arctic region. The main purpose of this study is a probabilistic analysis of atmospheric transport patterns from selected NRSs for the GIS-based studies of region's vulnerability and risk assessment of the NRS impact.

The NRSs of concern (in total 11) selected in this study are nuclear power plants located in Russia (Kola and Leningrad NPPs), Finland (Loviisa and Olkiluoto NPPs), Sweden (Barsebaeck, Oskarshamn, and Ringhals NPPs), Lithuania (Ignalina NPP), two groups of NPPs in the United Kingdom and Germany as well as the Novaya Zemlya test site (Russia). The geographical regions and countries of interest are the North and Central European countries and Northwest Russia.

Once the nuclear risk sites and geographical region of interest were defined, it is of particular interest to answer the following questions: Which geographical territories are at highest risk from the hypothetical accidental releases at selected NRSs? What are probabilities for radionuclide atmospheric transport to different neighboring countries in a case of accidents at these NRSs?

To answer these questions we applied several research tools developed within the "Arctic Risk" Project (*AR-NARP, 2001-2003; Baklanov & Mahura, 2001*). The first research tool is an isentropic trajectory model to calculate a multiyear (1991-1996) dataset of 5-day forward trajectories that originated over the NRS locations at various altitudes. As input data for modeling purposes we used NCAR meteorological gridded fields. The second research tool is a set of statistical methods (including exploratory, cluster, and probability fields analyses) for analysis of trajectory modeling results.

The results of probabilistic analysis of trajectory modeling results for 11 NRSs are presented as a set of various indicators of the NRS possible impact on geographical regions of interest. In this study, we calculated, constructed, and evaluated several indicators based on trajectory modeling results: 1) airflow, 2) fast transport, 3) maximum reaching distance, 4) maximum possible impact zone, 5) precipitation factor, and 6) typical transport time fields. To evaluate the temporal variability of all these indicators, an analysis was performed annually, seasonally, and monthly.

The NRS possible impact (on the concrete geographical region, territory, country, site, etc.) **due to atmospheric transport from NRS after hypothetical accidental releases of radioactivity <u>can be properly estimated</u> based on a combined interpretation of the indicators** (simple characteristics, atmospheric transport pathways, airflow and fast transport probability fields, maximum reaching distance and maximum possible impact indicators, typical transport time and precipitation factor fields) **for different time periods** (annual, seasonal, and monthly) **for any selected NRSs** (both separately for each site or grouped for several sites) **in the Euro-Arctic region**. Such estimation could be the useful input information for the decision-making process and planning of emergency response systems at risk sites of nuclear, chemical, biological, etc. danger.

It should be noted that the suggested probabilistic indicators of the risk site possible impact could be applicable for initial estimates of probability of atmospheric transport in the event of an accidental release at the risk sites and for improvement in planning the emergency response to radionuclide releases from the risk site locations. They are important input data for the social and economical consequences studies of the risk site impact on population and environment for the neighbouring countries as well as for the multidisciplinary risk and vulnerability analysis, and probabilistic assessment of the meso-, regional-, and long-range transport of radionuclides.

I. INTRODUCTION BACKGROUND

The risks of significant radioactive contamination and radiological consequences in geographical regions of concern are related to various nuclear risk sources located in the region of concern or adjacent territories. The contamination and consequences might be reflected on different scales – local, regional, global, and they might appear to be far reaching and of considerable concern for the whole Euro-Arctic region. Thus, it is of particular interest to answer the following questions:

- *Which sources appear to be the most dangerous for those living close to and far from these sources?*
- *Which geographical regions are at the highest risk from the hypothetical accidental releases on the nuclear risk sources in the Euro-Arctic region?*
- *What is the probability for radionuclide atmospheric transport to neighbouring countries or remote territories in a case of an accidental release from these sources?*

Baklanov & Mahura, 2001; Rigina & Baklanov, 2002 noted that for assessment of risk and vulnerability it is important to consider a set of various social-geophysical factors and probability indicators. These both depend on the geographical location of the area of interest and structure of its population. Thus, for estimation of the potential nuclear risk and vulnerability levels for the nuclear risk sites (NRSs) it will be important to know:

- *Which geographical regions are the most likely to be impacted?*
- *What are probabilities of the fast, average, and slow atmospheric transport from NRSs to neighbouring countries?*
- *What are precipitation probability and contribution during atmospheric transport for various atmospheric layers and over different geographical territories?*
- *What are temporal (annual, seasonal, and monthly) and spatial variability for the mentioned above characteristics?*
- *What are levels of contamination and consequences for the worst meteorological and accidental scenarios at NRSs?*
- *What is vulnerability to radioactive deposition with a focus on the transfer of certain radionuclides into food-chains especially native population and considering risk for different geographical areas?*
- *What are risk, socio-economical and geographical consequences for different geographical areas and population groups?*

The methodology by *AR-NARP, 2001-2003; Baklanov & Mahura, 2001; Baklanov et al., 2002a; Baklanov et al., 2002b; Baklanov et al., 2002c* mentioned several research tools and approaches, which could be applied for the probabilistic atmospheric studies. The developed methodological scheme consists of several major blocks or steps in research activities. The focus of this report will be only on the consideration of the trajectory modelling approach and statistical analysis of trajectory modelling results for the selected NRSs in the Euro-Arctic region (Table 1.1, Figure 1.1). Let us briefly consider research tools and approaches selected in this study that provide input data for the probabilistic risk and vulnerability studies, as well as constructing and evaluating various indicators of the NRS possible impact based on trajectory modelling results.

Research Tools and Approaches

The **first research tool** is the **trajectory modelling**. In our study, we applied an isentropic trajectory model based on a technique described by *Merrill et al., 1985*. A multiyear dataset of

forward trajectories originated over selected NRS locations (Table 1.1, Figure 1.1) at various altitudes above sea level (asl) was calculated. For the forward trajectory calculation, we used the National Center for Environmental Prediction (NCEP) Global Tropospheric Analyses (http://dss.ucar.edu/datasets/ds082.0/), which is one of the major gridded analyses available at the National Center for Atmospheric Research (NCAR, Boulder, Colorado, USA). The original dataset has resolutions of 2.5° x 2.5° latitude vs. longitude, and at 00 and 12 UTC (Universal Coordinated Time) terms. Although, in our study, we used this dataset, we should mention that any other datasets could be used too. For example, the DMI-HIRLAM high-resolution meteorological data (http://www.dmi.dk) or meteorological data from the European Centre for Medium-Range Weather Forecasts (ECMWF, Reading, UK) based on the ECMWF's global model forecast and analysis (http://www.ecmwf.int/services/data/archive/index.html). In a similar way, any other trajectory model could be used for the trajectory modelling purposes, for example, 3-D DMI trajectory model (*Sørensen et al., 1994*).

The **second research tool** is the **cluster analysis**. In this study, we did not present the results of the trajectory cluster analysis for all NRSs, because we consider this approach as the **simple approach**. The cluster analysis technique was applied in several studies related to the nuclear risk sites: at the Chukotka (*Mahura et al., 1997a; Jaffe et al., 1997a; Mahura et al., 1999b*), Kola Peninsula (*Mahura et al., 1997b; Jaffe et al., 1997b; Mahura et al., 1999a; Baklanov et al., 2001*) and Russian Far East (*Mahura, 2002*). The potential risk sources considered there were the nuclear power plants, spent nuclear fuel storage facilities, and nuclear submarine bases. In general, this technique allows identifying atmospheric transport pathways from NRSs (or any selected source points). In a similar way, it could be applied also to identify atmospheric transport pathways to the receptor points. In this case, the backward trajectories arrived at the sites will be used for the cluster analysis. This approach was applied in *Mahura et al., 1997a; Jaffe et al., 1997a; Mahura et al., 1999b.* More detailed analysis and interpretation of the backward trajectory clustering is described in the pilot study by *Mahura & Baklanov, 2002.*

The **third research tool** is the **probability fields analysis**. The first attempt to use the probability fields analysis to interpret atmospheric transport patterns was performed by *Mahura et al., 1997b; Jaffe et al., 1997b; Baklanov et al., 1998,* on example of the Kola NPP (Murmansk region, Russia). The major focus was the airflow probability fields which allowed to test the quality of the cluster analysis technique in identification of the general atmospheric transport pathways from NRS. Such probability fields analysis provides an additional information and detailed structure of the airflow patterns from the site on a geographical map. In this study, we evaluated annual, seasonal, and monthly probability fields for the airflow, fast transport, precipitation factor, and other indicators. These fields allow to identify the most impacted geographical regions.

Nuclear Risk Sites, Indicators of NRS Possible Impact, and Applicability of Results

The main focus of this report is to describe probabilistic analysis of results (based on the developed methodology for the probabilistic atmospheric studies by *Baklanov & Mahura, 2001*) for the further risk assessment of the selected – 11 - nuclear risk sites in the Euro-Arctic region. These sites include nuclear power plants (NPPs) in Russia, Lithuania, Germany, United Kingdom, Finland, and Sweden (see Table 1.1, Figure 1.1). All selected sites are located within the area of interest of the "Arctic Risk" Project. Moreover, the Kola NPP (Murmansk Region, Russia) has the old type of reactors (VVER-230); Leningrad (Leningrad Region, Russia) and Ignalina (Lithuania) NPPs have the RBMK type of reactor; and Novaya Zemlya (Novaya Zemlya Archipelago, Russia) was considered as a former nuclear weapons test site and potential site for nuclear waste deposit.

The Block of the British NPPs (BBP) is represented by a group of the risk sites: Chapelcross (Annan, Dumfriesshire), Calder Hall (Seascale, Cumbria), Heysham (Heysham, Lancashire), and Hunterston (Ayrshire, Strathclyde) NPPs and the Sellafield reprocessing plant. The Block of the German NPPs (BGP) is represented by a group of NPPs: Stade (Stade, Niedersachsen), Kruemmel (Geesthacht, Schleswig-Holstein), Brunsbuettel (Brunsbuettel, Schleswig-Holstein), Brokdorf (Brokdorf, Schleswig-Holstein), and Unterweser (Rodenkirchen, Niedersachsen). Although these NPPs use different reactor types and, hence, they could have different risks of accidental releases, the grouping is useful for airborne transport studies because all NPPs are located geographically close to each other and, hence, atmospheric transport patterns will be relatively similar.

Table 1.1. Nuclear risk sites selected for the "Arctic Risk" Project.

#	Site	Lat,°N	Lon,°E	Site Names	Country
1	KNP	67.75	32.75	Kola NPP	Russia
2	LNP	59.90	29.00	Leningrad NPP	Russia
3	NZS	72.50	54.50	Novaya Zemlya Test Site	Russia
4	INP	55.50	26.00	Ignalina NPP	Lithuania
5	BBP	54.50	-3.50°W	Block of the British NPPs	United Kingdom
6	BGP	53.50	9.00	Block of the German NPPs	Germany
7	LRS	60.50	26.50	Loviisa NPP	Finland
8	TRS	61.50	21.50	Olkiluoto (TVO) NPP	Finland
9	ONP	57.25	16.50	Oskarshamn NPP	Sweden
10	RNP	57.75	12.00	Ringhals NPP	Sweden
11	BNP	55.75	13.00	Barsebaeck NPP	Sweden
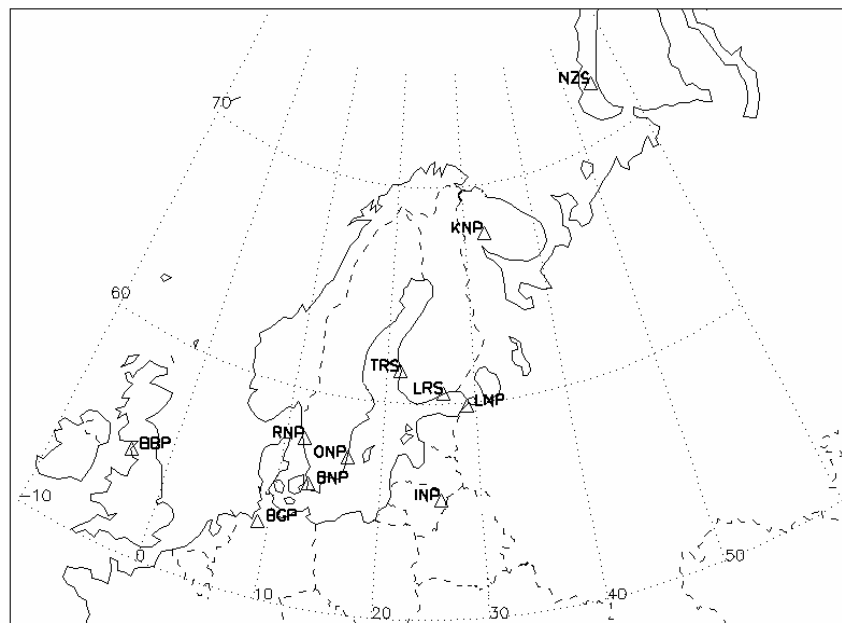
Figure 1.1. Nuclear risk sites selected for the "Arctic Risk" Project.

In this report, the results of probabilistic analysis for these sites are presented in a form of various indicators (Figure 1.2) of the NRS possible impact on selected geographical regions territories, and countries of concern (Figure 1.3). Among these indicators we should mention the following: 1) simple characteristics of the NRS possible impact, 2) atmospheric transport pathways

(ATP), 3) airflow (AF) probability fields, 4) fast transport (FT) probability fields, 5) precipitation factor (PF), 6) maximum reaching distance (MRD), 7) maximum possible impact zone (MPIZ), and 8) typical transport time (TTT) fields. The mentioned indicators are based on the interpretation of the trajectory modelling results. More detailed information (monthly, seasonal, and annual variability) for various NRS indicators is stored on CD (enclosed if ordered) and in Appendices.

CHARACTERISTICS AND INDICATORS OF NRS IMPACT

Simple Characteristics for Selected Geographical Regions:
- Upper & Lower Boundaries of NRS Impact
- Average Transport Time
- Atmospheric Transport by Layers
- Fast Transport, etc.

Atmospheric Transport Pathways (ATP)

Maximum Reaching Distance (MRD)

Maximum Possible Impact Zone (MPIZ)

Airflow (AF) Probability Fields

Precipitation Factor (PF)

Fast Transport (FT) Probability Fields

Typical Transport Time (TTT) Field

Other Characteristics and Indicators of NRS Possible Impact

Figure 1.2. Characteristics and indicators of the NRS possible impact.
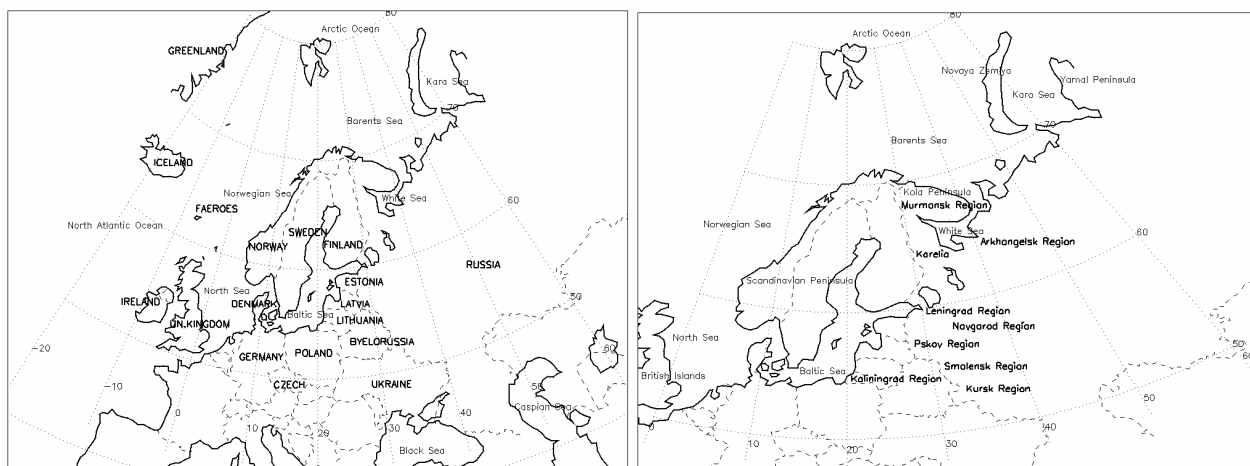
Figure 1.3. Geographical regions, territories, and countries selected for the "Arctic Risk" Project.

It should be noted that indicators of the NRS possible impact are applicable for initial estimates of probability of atmospheric transport in the event of an accidental release at NRSs and for improvement in planning the emergency response to radionuclide releases from the NRS locations. They are important input data for the social and economical consequences studies of the NRS possible impact on population and environment for the neighbouring countries as well as for the

multidisciplinary risk and vulnerability analysis, and probabilistic assessment of the meso-, regional-, and long-range transport of radionuclides.

Research Progress on the "Arctic Risk" Project

The methodological aspects and probabilistic analysis results for the dispersion modelling will be presented in the research reports by *Baklanov et al., 2002a* and *Mahura et al., 2003* as a subsequent part of the "Arctic Risk" Project. For this task, we applied the long-range transport - DERMA (*Sørensen, 1998; Baklanov & Sørensen, 2001*) and DMI-HIRLAM (*Sass et al., 2000*) models to simulate radionuclide transport for the hypothetical accidental releases at NRSs. Additional NRSs – Smolensk and Kursk NPPs (Russia), Chernobyl NPP (Ukraine), Forshmark NPP (Sweden), and Roslyakovo shipyard (Kola Peninsula, Murmansk Region, Russia) - were also included in the dispersion modelling to already initially selected 11 NRSs (as in Table 1.1) in the Euro-Arctic region.

The results of these both parts (based on trajectory and dispersion modelling approaches) in the "Arctic Risk" Project (*AR-NARP, 2001-2003; Mahura et al., 2002c; Mahura et al., 2003*) will be used into two ways. First, these results will be used in evaluation of vulnerability to radioactive deposition (concerning its persistence in the ecosystems with focus to transfer of certain radionuclides into food chains of key importance for the intake and exposure in a whole population and certain groups of the Nordic countries) applying approach by *Bergman, 1999*. Second, these results will be used also for risk evaluation and mapping using demographic databases in combination with the GIS-analysis as described by *Rigina & Baklanov, 1999; Rigina, 2001; Rigina & Baklanov, 2002*. Their approach was applied to analyse socio-economical consequences for different geographical areas and population groups taking into account various social-geophysical factors and probabilities.

II. PROBABILISTIC ANALYSIS OF ATMOSPHERIC TRANSPORT PATTERNS FROM NRSs IN EURO-ARCTIC REGION

In this report we will present and discuss some results based on application of the methodology for the probabilistic assessment of the nuclear risk sites impact suggested by *Baklanov & Mahura, 2001*. The nuclear risk sites of concern in this study are eleven sites located in the Euro-Arctic region (shown in Table 1.1). For this purpose we used calculated trajectories (during 1991-1996) originated over selected NRSs to construct and estimate various indicators of the NRS possible impact based on the trajectory modelling approach.

In §2.1 of this report, on example of the Kola NPP (Murmansk Region, Russia), the simple characteristics of the NRS possible impact and atmospheric transport pathways from the site are show. Detailed evaluation of these is given by *Mahura et al., 1997b; Jaffe et al., 1997b; Mahura et al., 2001*. In further sections, additional indicators – all based on the trajectory modelling results - of the NRS possible impact, such as airflow probability field (§2.2), fast transport probability field (§2.3), maximum reaching distance and maximum possible impact zone (§2.4), typical transport time field (§2.5) are considered for 11 NRSs. The precipitation factor (§2.6) field will be shown only for the Kola NPP, because a new dispersion modelling approach in evaluation of the wet deposition patterns (*Baklanov et al., 2002a; Baklanov et al., 2002c*) could provide more representative information about possibility of the radionuclide removal during atmospheric transport from the accident location.

2.1. *SIMPLE CHARACTERISTICS OF NRS IMPACT AND ATMOSPHERIC TRANSPORT PATHWAYS*

In general, we analyzed all calculated forward trajectories that originated over the NRS locations to investigate the likelihood that the nuclear risk sites might have impact on the neighbouring countries or distant geographical regions. As a first approximation, trajectories can be separated into groups by altitudes of initial trajectory points. The boundaries of geographical regions can be selected depending on political borders, climatic regimes, areas of research interest, etc. For simplicity, we assumed that any trajectory, which crosses into the boundaries of the chosen geographical region, might bring air parcels containing radionuclides. Therefore, only trajectories crossing boundaries of these regions should be selected in further evaluation of the NRS impact.

Among the **simple characteristics** we could suggest the following. First, it is the number and percentage of trajectories reaching the boundaries of the chosen geographical regions. Second, it is the number and percentage of days when, at least, one trajectory had reached the region. Third, it is the average transport time of air parcels to reach chosen regions. Fourth, it is the probability of atmospheric transport within different atmospheric layers (boundary layer and free troposphere). Fifth, it is the likelihood of very rapid (fast) atmospheric transport of air parcels, i.e. transport in one day or less. All these characteristics can be evaluated over a multiyear dataset of calculated trajectories, by individual year, season, and month. Such analysis allows to investigate possible spatial and temporal variation in the airflow patterns from the NRS region to neighbouring countries or selected geographical regions of concern.

Another approach in the simple analysis is to apply, as a research tool, a **cluster analysis** technique for trajectories originated at each site. As a result of this analysis, the mean trajectories for each cluster will be produced. These mean trajectories are **atmospheric transport pathways** from the sites, and they can be explained based on existing synoptic features and peculiarities in the

studied regions. These pathways show the general direction of atmospheric transport from the site region as well as probability of such transport (an example is shown in Figure 2.1.1). The mean trajectory for each cluster is given with points indicating 12-hour intervals. Two numbers are used for each cluster. The first is the identifier of a cluster. The second is the percentage of trajectories within a cluster. The cluster numbers are arbitrary and only used to separate the possible types of transport.
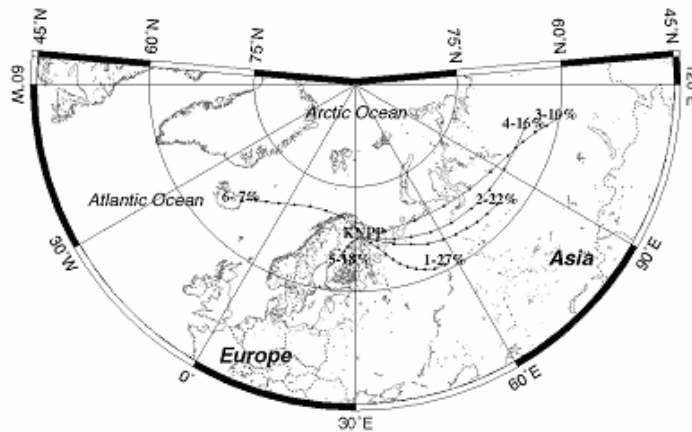
Figure 2.1.1. Annual atmospheric transport pathways from the Kola NPP region.

For the Kola NPP, six clusters were identified for the 5-day trajectories originating over the NRS region within the boundary layer. Four of them (#1, 2, 3 and 4 with 27, 22, 10 and 16% of occurrence, respectively) show westerly flow. These were observed about 75% of the time. Cluster #6 (7%) was used to show the possibility of the easterly flow toward the North Atlantic. Cluster #5 (18%) represents transport to the southwest through the Scandinavian Peninsula into the Baltic Sea. The westerly flows are predominant throughout the year. Cluster analysis of trajectories by seasons showed that atmospheric transport from the west varies from 68% (in fall) to 94% (in spring) of the time. Transport from the east occurs from 3% (in winter) to 26% (in summer) of the cases. Transport in the southern direction takes place 15% of the time (in winter) increasing up to 25% (in fall). Analysis of trajectories at higher altitudes (1.5 and 3 km asl) showed that in the free troposphere the probability of atmospheric transport from the west increases up to 90%.

Although results of the cluster analysis are useful, they are not completely representative, because information between clusters represented by mean trajectories (or transport pathways), reflecting only the general direction of airflow from the site, is "missing". Therefore, another research tool (discussed in §2.2) – probability fields analysis - is required to extract this additional information. It should be noted that some examples in evaluation of simple characteristics and atmospheric transport pathways from the sites based on cluster analysis of trajectories are discussed for the Northwest Russia and Russian Far East nuclear risk sites by *Mahura et al., 1999a; Mahura et al., 1999b; Baklanov et al., 2001; Mahura, 2002*.

2.2. AIRFLOW PROBABILITY FIELDS

Probabilistic analysis is one of the ways to estimate the likelihood of occurrence of one or more phenomena or events. In this study, for each NRS we calculated a large number of isentropic forward trajectories that passed over various geographical regions. Each calculated trajectory contains information about longitude, latitude, altitude, pressure, temperature, relative humidity, etc. at each 12-hours interval. The probability fields for these mentioned characteristics, either

individual or combined, can be represented by a superposition of probabilities for air parcels reaching each grid area in the chosen domain or on a geographical map.

Approaches to Construct Probability Fields

Let us consider in more details several common approaches to construct probability fields based on trajectory modelling results (*Baklanov & Mahura, 2001; Mahura, 2001*). For all approaches, initially, we construct a gridded domain having M_{lat} x M_{lon} latitude vs. longitude grid points with a size of ΔY x ΔX degrees latitude vs. longitude. The selection of sizes ΔY and ΔX depends on the resolution of original meteorological fields used for trajectory calculation purposes. The number of latitudinal and longitudinal grid points - M_{lat} and M_{lon} – is selected taking into account the farthest geographical boundaries which might be reached by air masses during the year.

The **first approach** to construct such fields (an example is shown in Figure 2.2.1a) considers the number of trajectory intersections with each cell of the gridded domain ($N_{CELL_{ij}}$):

$$N_{CELL_{ij}} = \sum_{k=1}^{N_{tr}} \sum_{j=1}^{M_{lat}} \sum_{i=1}^{M_{lon}} n_{ijk} \quad,$$

$$n_{ijk} = \begin{cases} 0 \\ 1 \end{cases} \quad if \quad \begin{cases} X_i \le X_{k,t} < X_{i+1} \\ Y_j \le Y_{k,t} < Y_{j+1} \end{cases},$$

where:

$Y_{k,t}$, $Y_{k,t}$ – longitude and latitude of *k*-trajectory at time *t* (where: $t = 0,5$ days; $\Delta t = 12$ hours);
X_i, X_{i+1} – longitudinal boundaries of the grid cells of domain;
Y_j, Y_{j+1} – latitudinal boundaries of the grid cells of domain;
N_{tr} – total number of trajectories during the multiyear period studied (number days per year $*$ 8 trajectories per day $*$ number of years);
M_{lat}, M_{lon} - number of the grid points in domain along latitude and longitude.

The isolines (shown in Figure 2.2.1a) start from 25 intersections of trajectories with cells of the gridded domain (maximum isoline represents 750 and more intersections), and all other isolines are selected arbitrary, although these used to reflect the dominance of the westerly atmospheric transport from the site as well as the fact that the airflow, in general, is concentrated around the site.

| (a) | (b) | (c) |
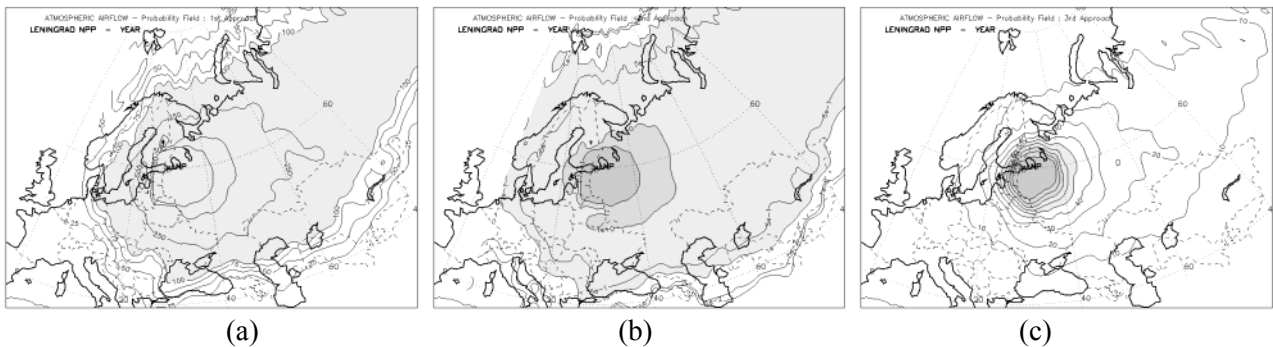
Figure 2.2.1. Examples of airflow probability fields for the Leningrad NPP (LNP) using the a) first, b) second, and c) third approaches to construct probabilistic fields based on trajectory modelling results.

The **second approach** for construction of probabilistic fields (Figure 2.2.1b) uses an assumption that the total sum of contributions from all individual grid cells of domain is equal to 100%. Hence, the contribution or probability that a given trajectory might reach the geographical boundaries of the individual cell could be estimated as follows:

$$P_{i,j} = \frac{N_{CELL_{ij}}}{N_{tot}} \cdot 100\%,$$

$$N_{tot} = \sum_{i=1}^{M_{lat}} \sum_{j=1}^{M_{lon}} N_{CELL_{i,j}},$$

where:

$P_{i,j}$ - probability of trajectory intersections with a particular cell of the gridded domain;

N_{tot} – total number of trajectory intersections with all cells of the gridded domain.

The isolines (shown in Figure 2.2.1b) start from the smallest – "1e-2" (%) - contribution of cells into the total redistribution of the airflow from the site. In vicinity of the site and on the regional scale up to 1000 km the contribution of cells varies from 7 to 1%. The contribution of more distant cells from the site decreases by orders of magnitude. Similarly to Figure 2.1.1a, this probabilistic field also reflects the dominance of the westerly atmospheric flows from the Leningrad NPP region as well as concentration of the airflow around the site.

The **<u>third approach</u>** for construction of probabilistic fields (Figure 2.2.1c) uses an assumption that for an individual NRS there is always an area where there is the highest probability of the maximum possible impact due to atmospheric transport. The borders of such an area (or more precisely, the cells included in such area) could be estimated by comparing the number of trajectory intersections with the cells (adjacent to the NRS location) with the cell where the maximum number of intersections occurred: $N_{AMC} = \max(N_{CELL_{1,1}}, ..., N_{CELL_{Mlatt,Mlon}})$. Among all grid cells, the cell where the absolute maximum of intersections occurred will be identified as an "absolute maximum cell" (AMC). Because all trajectories start near the NRS region, to account for the contribution into the flow at larger distances from the site, we extended the area of maximum to cells adjacent to the AMC. We compared the number of intersections in cells adjacent to AMC and then assigned additional cells, which had difference of less than 10% between cells. Therefore, this new "area of maximums", if isolines are drawn, will represent the area of the highest probability of the possible impact (AHPPI) from NRS. Assuming a value of 100% for this area, the rest could be re-calculated as percentage of the area at the highest probability of the possible impact, or:

$$P_{AHPMI_{i,j}} = \frac{N_{CELL_{ij}}}{N_D} \cdot 100\% ,$$

$$N_D = N_{tot} - N_{AHPMI} ,$$

$$N_{AHPMI} = \sum_{j=1}^{M_{lat}} \sum_{i=1}^{M_{lon}} n_{ij} ,$$

$$n_{ij} = \begin{cases} 0 \\ N_{CELL_{i,j}} \quad if \quad N_{CELL_{i,j}} \geq 0.9 \cdot N_{AMC} \end{cases},$$

where:

$P_{AHPMI_{i,j}}$ - probability of the NRS impact with respect to the area of the highest probability of the possible impact (AHPPI) of the nuclear risk site;

N_D - total sum of trajectory intersections with cells from the gridded domain, except the cells located in the boundaries of AHPPI for the nuclear risk site;

N_{AHPMI} – total sum of trajectory intersections with cells from the gridded domain located within the boundaries of AHPPI for the nuclear risk site.

The isolines (shown in Figure 2.2.1c) start from "10" (%) and show contribution of cells into the total redistribution of the airflow around the site with respect to AHPPI. The boundaries of

AHPPI (extended in east-south sector from the site) are shown by the isoline of ">90" (%). This field also shows dominance of the westerly flows from the NRS region.

In our study, we selected the third approach to construct the probabilistic fields as the most representative to evaluate the NRS possible impact. We should note that the most interest for the further analysis would be the following types of probabilistic fields: a) airflow, b) fast transport, c) maximum reaching distance, d) maximum possible impact zone, e) typical transport time, and f) precipitation factor.

Airflow Probability Fields for NRSs in the Euro-Arctic region

The **first type of probabilistic fields** - **airflow probability fields** - shows the common features in the atmospheric transport patterns from NRSs. First, it could provide a general insight on the possible main direction of the radioactive plume transport. Second, it shows a probability that radioactive plume will reach or pass over a given area on a geographical map. In comparison with the atmospheric transport pathways (an example is shown in §2.1), the AF probability fields show more detailed information about distribution of direction and probabilities of atmospheric transport from the sites toward a concrete geographical territory, region, country, or site.

|		
(LNP)	(KNP)	(INP)
(BBP)	(BGP)	(BNP)
(LRS)	(TRS)	(ONP)
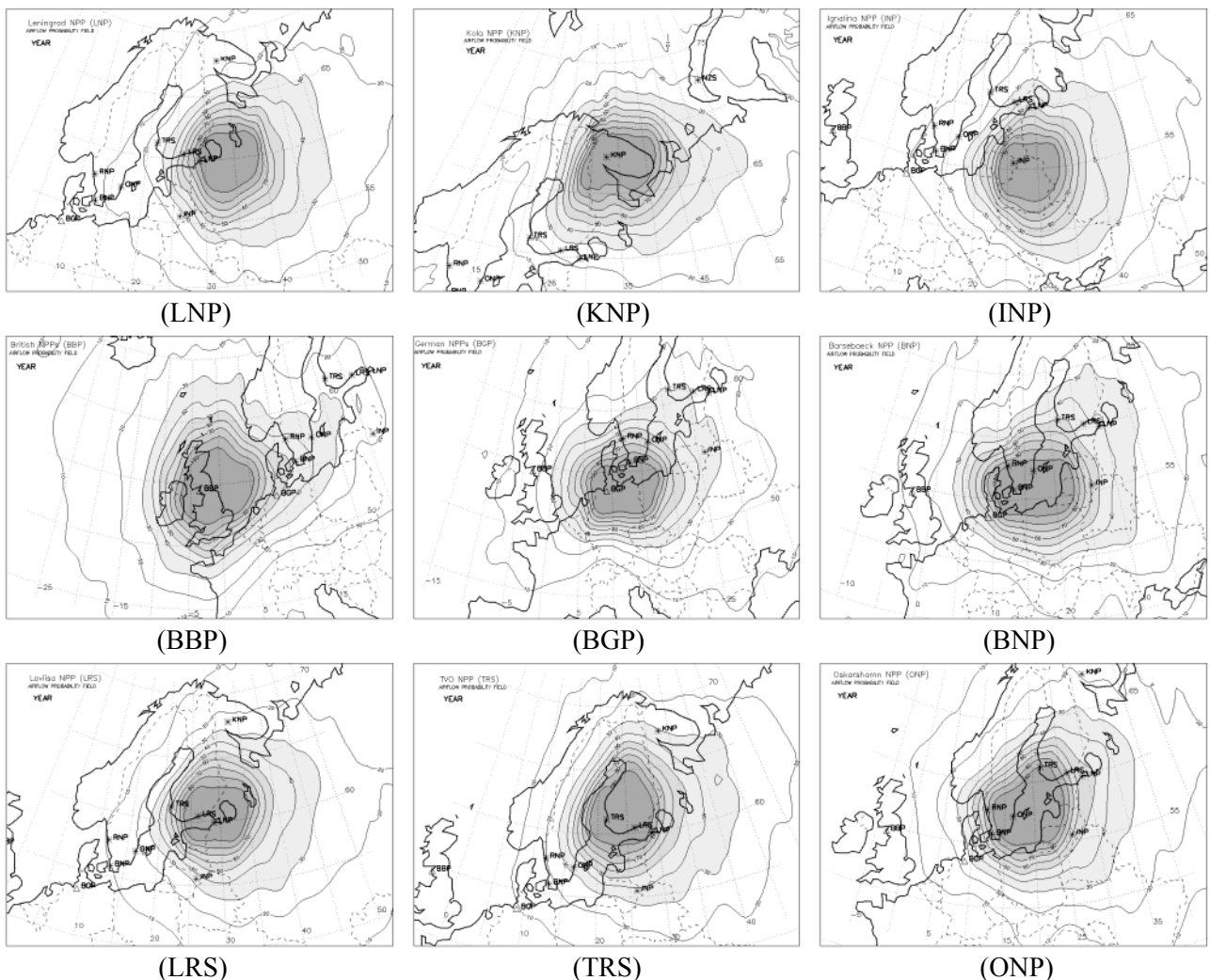
Figure 2.2.2. Annual airflow probability fields for the selected NRSs in the Euro-Arctic region.

Moreover, airflow probability field is a reliable test to reject or support results of the cluster analysis (which could be applied to identify the general atmospheric transport pathways from

12

NRSs), because the calculated clusters (or mean trajectories) will be located in the troughs and crests of probabilistic fields. The regions, where the highest crossing by trajectories is occurred, have the highest probability of the NRS possible impact. In this study, all airflow probability fields were constructed by averaging airflow patterns over a selected time period: year, season, and month (based on a multiyear dataset). The annual (see Figure 2.2.2), monthly (see Appendix 1), and seasonal variability of the airflow probability fields for the selected NRSs is stored on CD (enclosed if ordered).

For example, on an annual scale, for both Kola NPP (KNP) and Leningrad NPP (LNP), there is a clear dominance of the westerly flows in the atmospheric transport from the sites (Figure 2.2.2). The AHPPIs of these sites are extended in the eastern direction, although for the Kola NPP there is an extension of AHPPI to the south-west of the site. For the Kola NPP, it is also reflected by the cluster analysis of trajectories where cluster #5 (18% of the time as shown in Figure 2.1.1) lies in the same direction. As any meteorological variable, the AF probability fields calculated based on the wind characteristics have a temporal variability.

| (Spr) | (Sum) |
| (Fal) | (Win) |
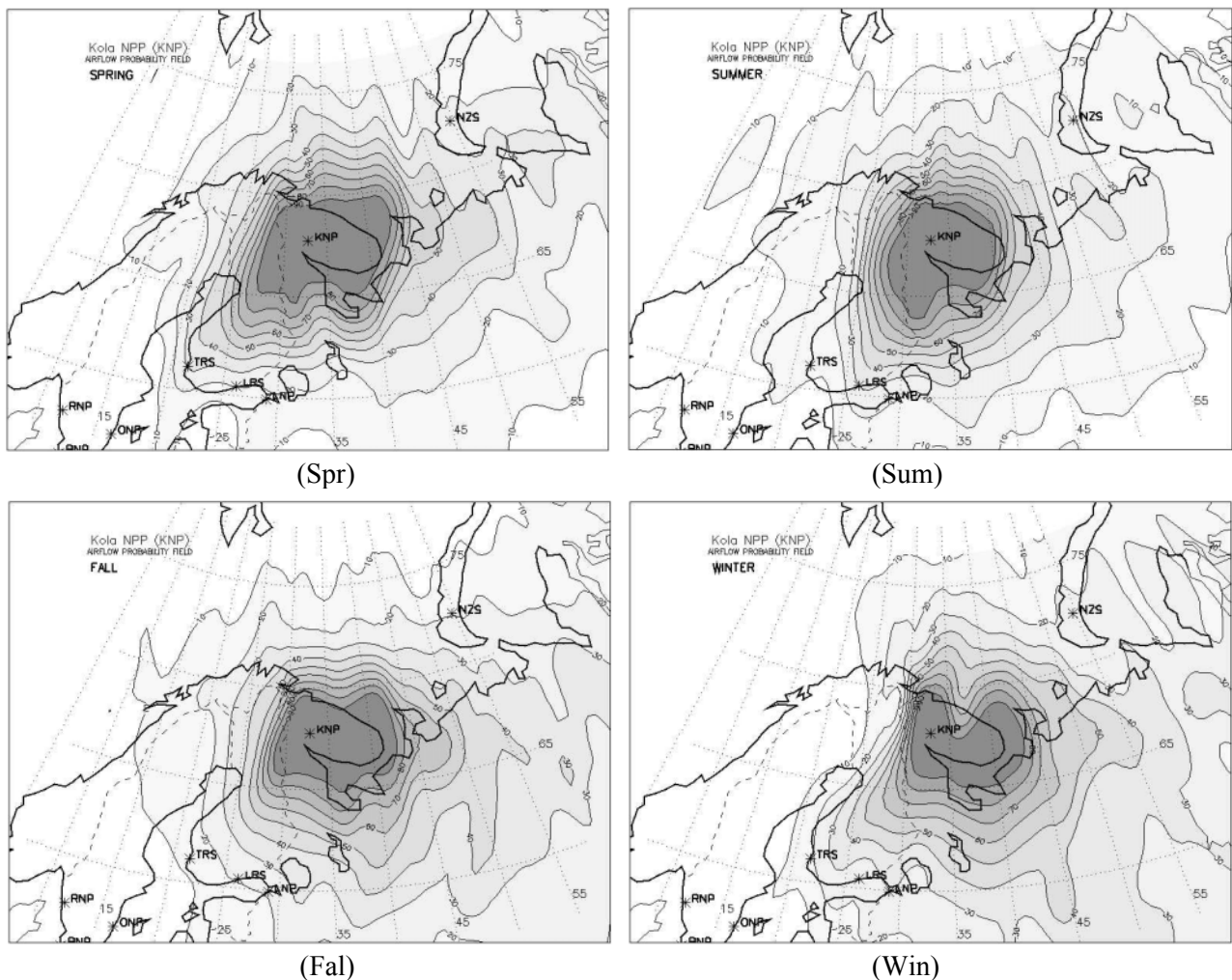
Figure 2.2.3. Seasonal airflow probability fields for the Kola NPP (KNP).

Let us consider, as an example, the variability of the airflow patterns for the Kola NPP by seasons (Figure 2.2.3) and for the Leningrad NPP by months (Figure 2.2.4). For the Kola NPP, during all seasons, the predominant transport is in the eastern direction from the site. Although, during spring, there is increase of transport in the south-western direction, and it is reflected by shifting of the AHHPI boundaries to the central territories of Finland (Figure 2.2.3a). During

summer, it is extended to the south of the site (reaching 65°N), but in other seasons it is located northerly of this latitude. During winter, the probability to reach Sweden is minimal; but the north-western and central regions of Russia are at the higher risk of being impacted during atmospheric transport from NRS. Moreover, it should be noted, that isolines of the airflow probability fields could be represented as the varying boundaries showing an order of the NRS possible impact on the concrete geographical territory. For example, for the Yamal Peninsula (Russia), likelihood of the NRS possible impact is the lowest during summer in comparison with other seasons, and for the Baltic States this likelihood is the lowest during spring.

(Jan)	(Feb)	(Mar)
(Apr)	(Mar)	(Jun)
(Jul)	(Aug)	(Sep)
(Oct)	(Nov)	(Dec)
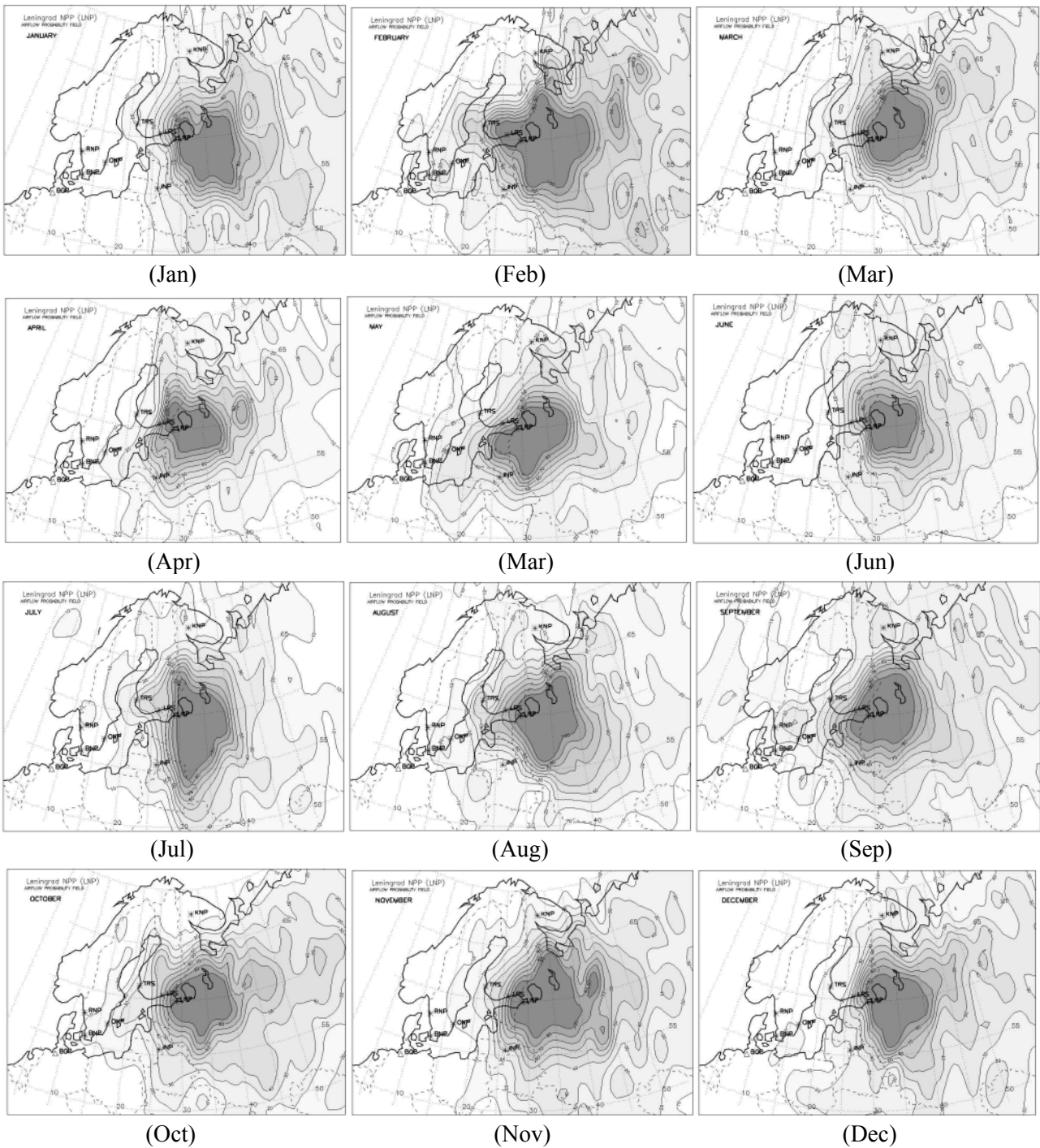
Figure 2.2.4. Monthly airflow probability fields for the Leningrad NPP (LNP).

For the Leningrad NPP, more detailed consideration of temporal variability by months (Figure 2.2.4) shows some peculiarities in the airflow patterns, which are not seen on both annual and seasonal scales. During July, atmospheric transport in the southern direction dominates for trajectories originated within the boundary layer over the Leningrad NPP region. The AHPPI boundaries reach territories southerly of 55°N. During February and March, the boundaries are extended significantly to the west of the site. During October and November, the probability for air parcels to pass over the Barents Sea is decreased. During September, there is a probability to reach the western seashore of the Southern Norway, although during other months, only a small part of the northern territories of the country might be affected by the Leningrad NPP. Throughout the year, the boundaries of the LNP AHPPI are located within the Russian territories, except during March, September, and November when they are extended also to the northern territories of Estonia.

It should be noted that the westerly transport dominates for all NRSs considered in this study. Although, for example, for the block of the British NPPs (BBP), Oskarshamn NPP (ONP), and Olkiluoto NPP (TRS), the airflow pattern is shifted toward the northeast of the site. For the Ignalina NPP (INP), the AF probability field is shifted toward the southeast of the site. For NRSs located closer to the North Atlantic Ocean region (i.e. blocks of the British (BBP) and German (BGP) NPPs, and Barsebaeck NPP (BBP)), the boundaries of probabilistic fields are extended farther (approximately on 1/3 in comparison with other NRSs) in the western direction from the sites. Therefore, the probability to reach more remote (in the western direction) territories from the sites is increased.

We should note that the airflow probability fields could be used for emergency planning and preparedness, in advance, for estimates of possible atmospheric transport (including probabilities, direction, speed, etc.) of the radionuclide cloud after hypothetical accidental releases at NRSs.

2.3. FAST TRANSPORT PROBABILITY FIELDS

The **second type of probabilistic fields** - **fast transport probability fields** - indicates the probability of the air parcels movement during the first day of transport. It is important information, especially, for the impact estimating of the short-lived radionuclides such as ^{133,131}I, ^{132}Te and Noble gases such as ^{85}Kr, ^{131,133,135}Xe. These fast transport fields show those territories that may be reached after the first 12 and 24 hours of atmospheric transport from the site, and those areas that are at the most danger due to fast transport. In this study, the fast transport probability fields were calculated after 12 and 24 hours of atmospheric transport from the risk sites.
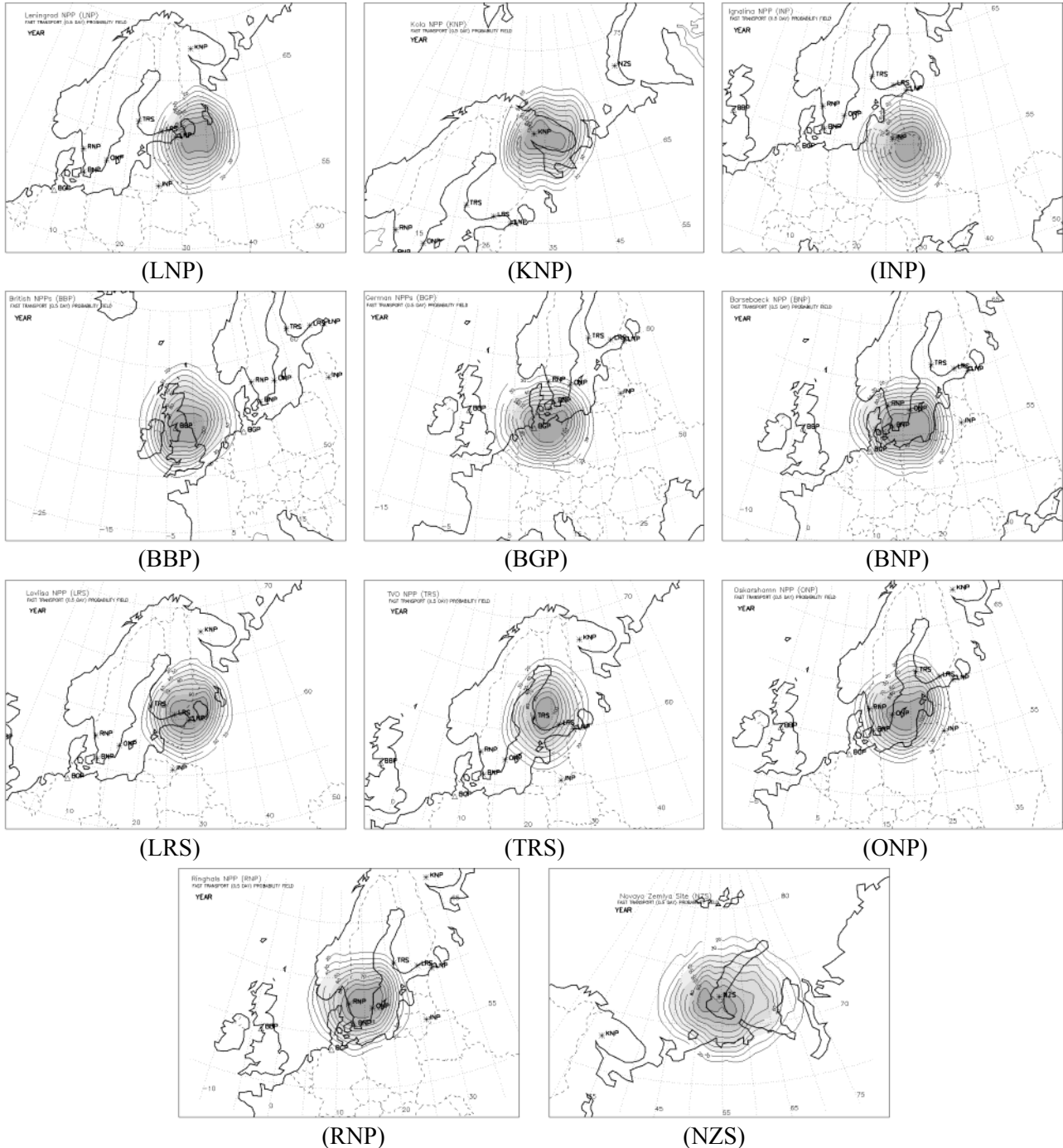
The fast transport probability fields characterize not only the highly possible direction of the radionuclide cloud atmospheric transport from the risk sites, but also define boundaries of territories on a geographical map where the order of the NRS possible impact could be evaluated. In this case, it is possible to depict the region (i.e. AHPPI) on a map where the risk site impact might be the highest, and for other regions to re-calculate the NRS possible impact as a part of NRS AHPPI.

The annual FT probability fields at both terms (12 and 24 hours) are presented for the selected NRSs in the Euro-Arctic region in Figures 2.3.1 and 2.3.2, respectively. The seasonal and monthly variability of these fields is stored on CD (enclosed if ordered) and in Appendices 2 and 3.

Let us consider several examples of result interpretation. First, it is an individual interpretation of the airflow or/and fast transport probability fields for one or more NRSs with respect to geographical regions, territories, or countries of concern. Second, it is a combined interpretation of the airflow and fast transport probability fields for two or more NRSs with respect to each other and geographical regions, territories, or countries of concern.

Individual Interpretation of Airflow/Fast Transport Probability Fields for One NRS

Let us consider some NRSs for such analysis. For the Kola NPP (KNP), the annual FT probability field after 12 hours of atmospheric transport (Figure 2.3.1) shows, as it is expected, that the entire Kola Peninsula is located within the area of the highest probability of the possible impact (AHPPI) from NRS. During the first 12 hours, the atmospheric transport from KNP is dominated by westerlies, although after 24 hours the transport to southwest can be also identified (Figure 2.3.2).

(LNP)	(KNP)	(INP)
(BBP)	(BGP)	(BNP)
(LRS)	(TRS)	(ONP)
(RNP)	(NZS)	

Figure 2.3.1. Annual fast transport probability field after 12 hours of atmospheric transport from the selected NRSs in the Euro-Arctic region.

Two maxima of AHPPI could be seen. The first is located in the eastern part of the Kola Peninsula, second − in the central regions of Karelia and Finland. Both of these show that after a

day of transport, there is the highest possibility that the radionuclide cloud will arrive to the mentioned territories, and hence, the NRS possible impact might be higher compared with other regions.
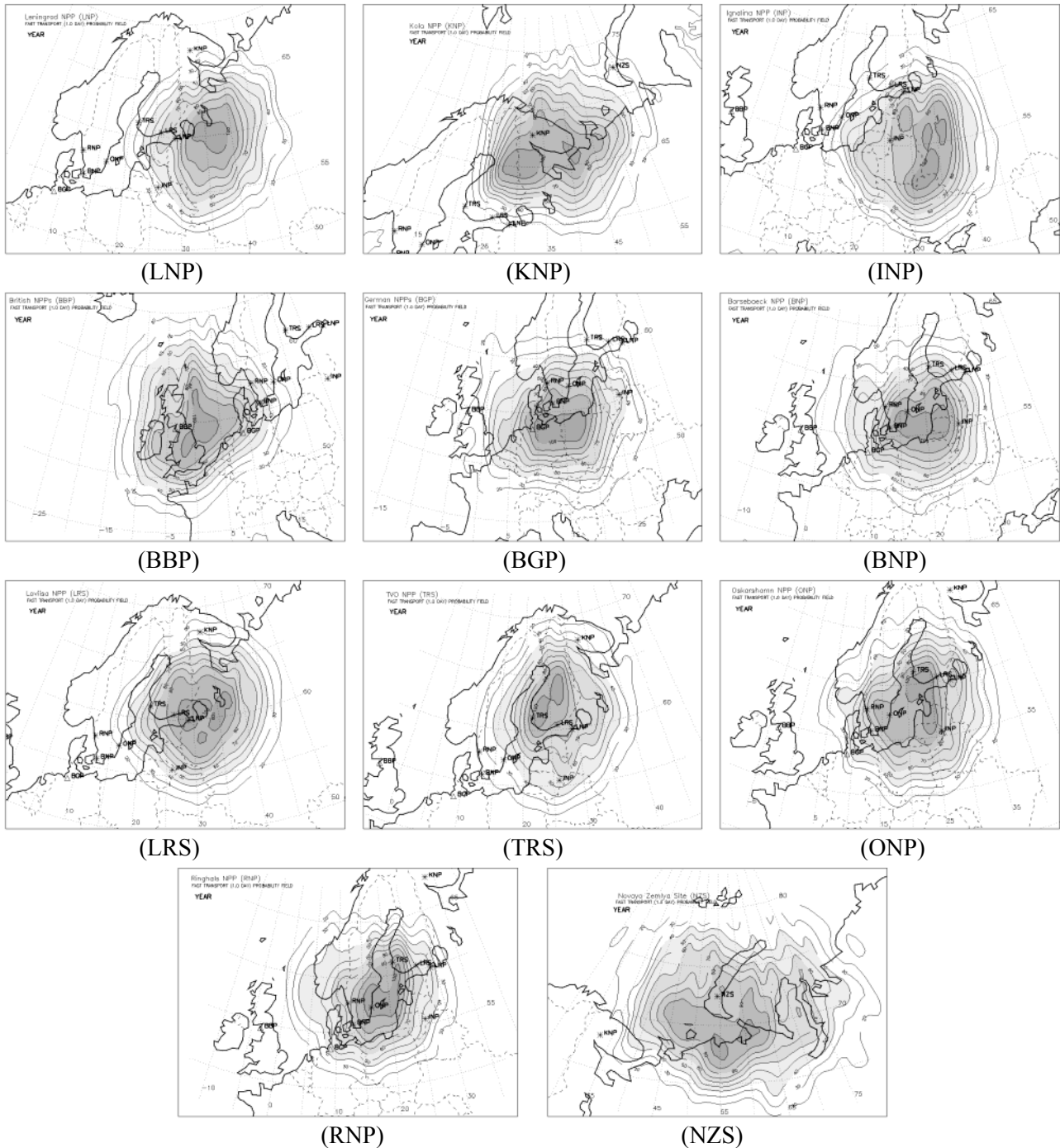
Figure 2.3.2. Annual fast transport probability field after 24 hours of atmospheric transport from the selected NRSs in the Euro-Arctic region.

On a seasonal scale, for the Kola NPP (Figure 2.3.3), during fall the FT probability field after 24 hours shows the shift of AHPPI in the eastern direction from the site toward less populated territories of the Northwest Russia. During summer, the total area of the fast transport fields is decreased (due to significant decrease of wind speeds during summer compared with other seasons).

This tendency is observed for all NRSs. In the same time, more southern regions with respect to the Kola NPP are included in the boundaries of AHPPI. There are also several maxima of AHPPI in other seasons compared with summer.

For the Novaya Zemlya Test Site (NZS), where in the Former Soviet Union the testing of nuclear weapons was conducted, on an annual scale, there is a pattern showing transport in the western direction at the end of the first 12 hours of atmospheric transport (Figure 2.3.1), and a pattern showing transport in the southern direction at the end of the first day of atmospheric transport (Figure 2.3.2). We should note that for the FT probability field after 12 hours, the AHPPI, although it is located near the site, is separated into two maxima: one to the east and one to the west of the site. After the first day, the NRS possible impact will be the highest on the territories of the Russian Arctic seashore. Moreover, there are also two maxima of KNP AHPPI, but they are located to the south of the site.

(Spr)

(Sum)

(Fal)

(Win)
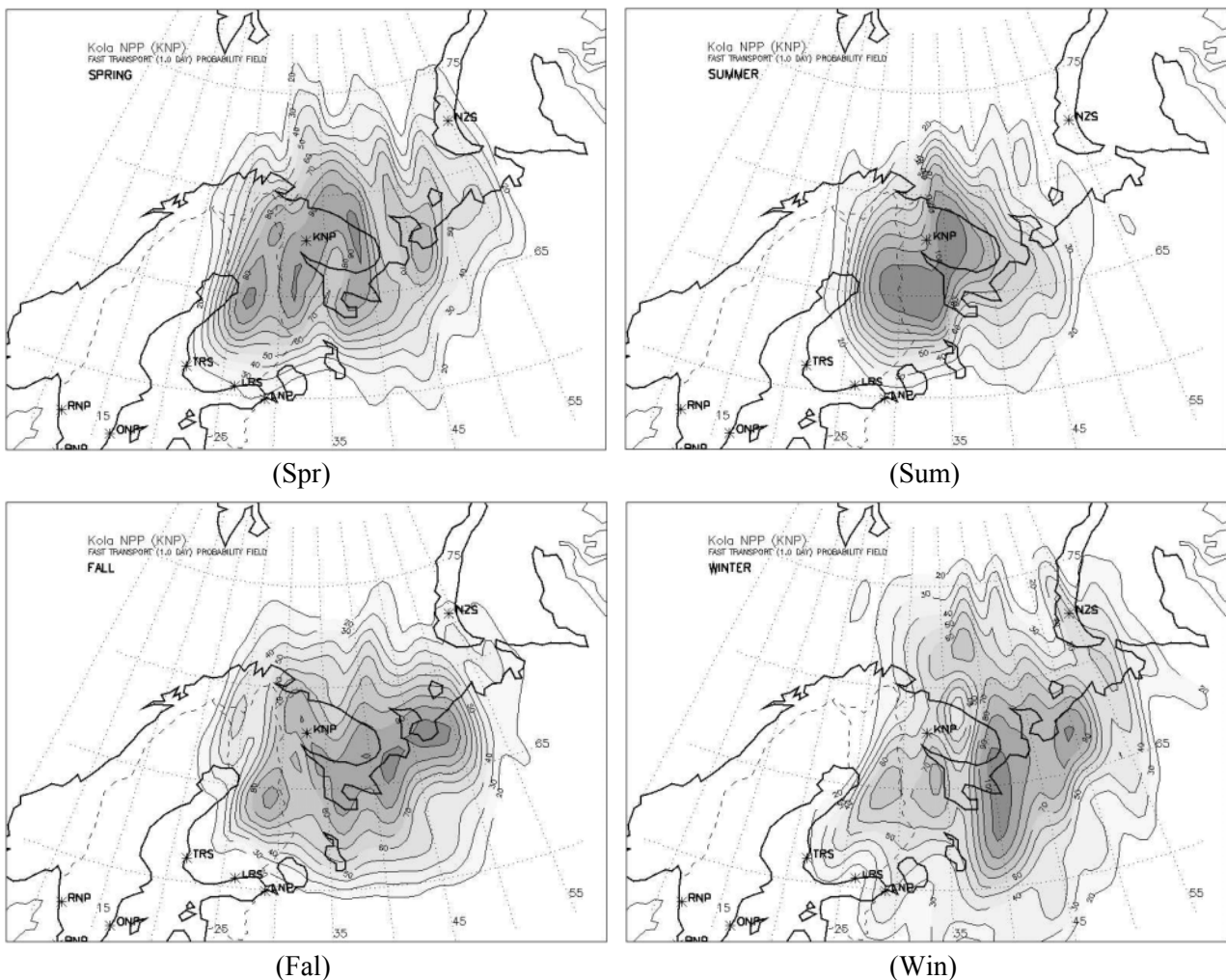
Figure 2.3.3. Seasonal variability of the fast transport probability fields after 24 hours of atmospheric transport for the Kola NPP (KNP).

Let us compare the NRS possible impact from two or more NRSs on the concrete country of concern – 1) Denmark and 2) Kaliningrad Region (Russia). For this purpose, for simplicity, we will evaluate the annual (although seasonal or monthly variability could be used) fast transport probability fields after 12 and 24 hours of atmospheric transport for 1) the blocks of the British (BBP) and German (BGP) NPPs (as example 1); the Ignalina (INP) and Barsebaeck (BNP) NPPs (as example 2). Such analysis could allow determining: which of NRSs, from the probabilistic point

of view, represents the highest danger due to atmospheric transport to the concrete geographical region, territory, country, site, etc.

In the first example, for both blocks of NPPs – German (BGP) and British (BBP), during the first 12 hours, the tendency in dominating of westerly flows is observed (Figure 2.3.1). The area of BGP AHPPI is higher compared with area of BBP AHPPI. The boundaries of the AHPPI's middle and high values (>50%) reaches the central and southern territories of Denmark. For the British NPPs, the maximal values of AHPPI are located in a vicinity of the British Islands, and probability to reach the Danish territories is minimal. The fast transport probability fields after 24 hours show (Figure 2.3.2), that although the dominating atmospheric transport for both BBP and BGP sites is still toward the east, for block of the British NPPs the transport toward the southern and northern direction could be observed. The BBP AHPPI area is increased significantly, and its boundaries are extended farther in the meridional direction compared with latitudinal direction. Hence, the probability to reach the western territories of Denmark had risen.

In the second example, for both NRSs – Ignalina (INP) and Barsebaeck (BNP) NPPs – the westerly flows had dominated during the first 12 hours of atmospheric transport (Figure 2.3.1). But for INP, at the end of the first day there is a tendency in shifting of the airflow in the south-eastern direction. For BNP, the western territories of the Kaliningrad Region will be located within the AHPPI boundaries. Moreover, the entire Kaliningrad Region, Lithuania, and Latvia are located inside the BNP AHPPI after 24 hours of atmospheric transport (Figure 2.3.2). Although, for the Ignalina NPP, the medium values of INP AHPPI will be only on the eastern territories of the Kaliningrad Region.
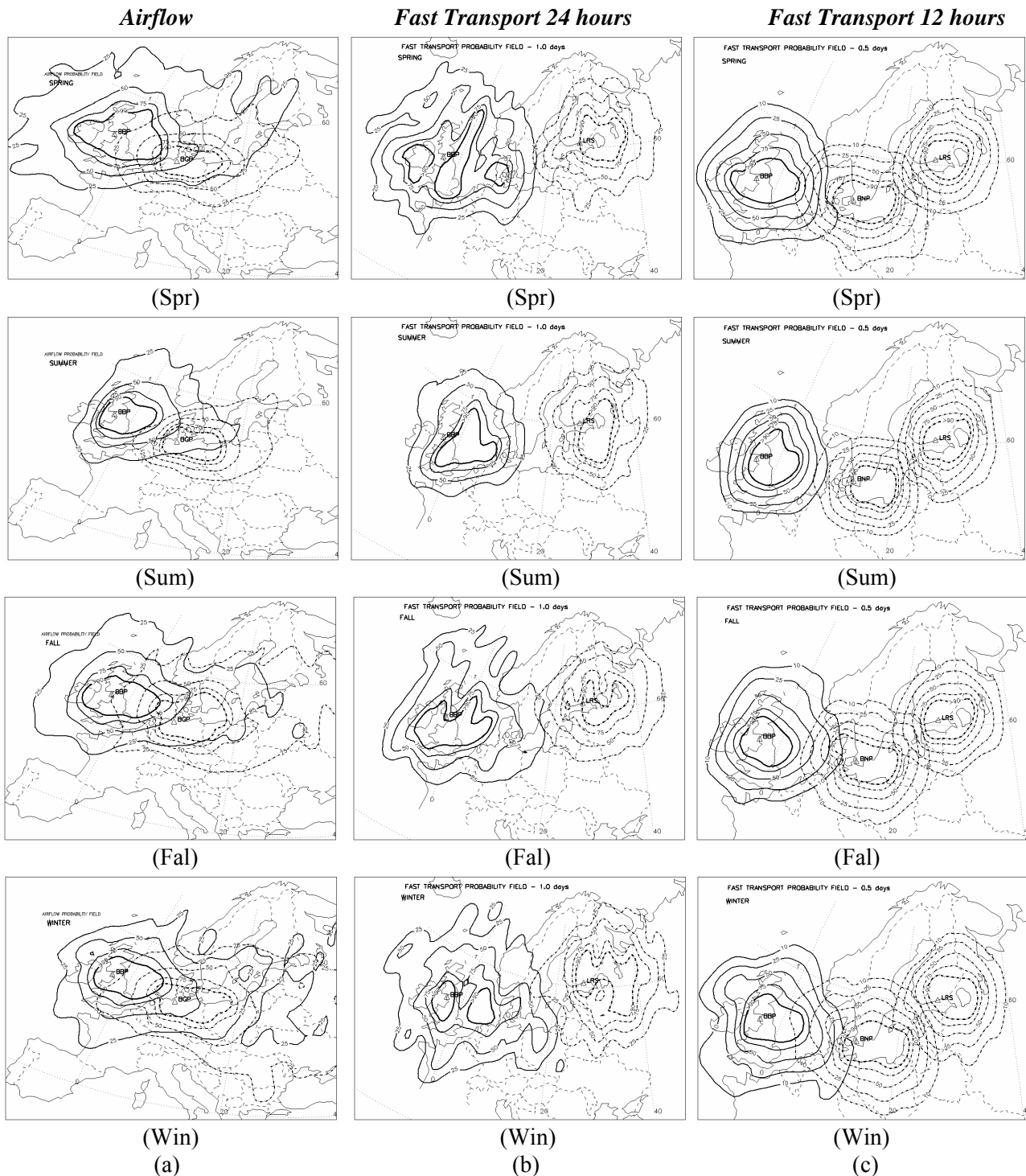
Combined Interpretation of Airflow/Fast Transport Probability Fields for Several NRSs

Let us consider the combined analysis of the AF and FT probability fields for several NRSs (examples are shown in Figure 2.3.4). We will compare the seasonal variability in the airflow and fast transport patterns for the blocks of the British (BBP) and German (BGP) NPPs, Loviisa (LRS) and Barsebaeck (BNP) NPPs with respect to the Nordic countries – Denmark, Finland, Norway, Sweden, Iceland, and Faeroes Islands. It is a convenient step for such analysis to plot a selected field on one figure for several NRSs simultaneously, and to choose several critical isolines (for example, 10, 25, 50, 75, >90 % of NRS AHPPI) for better interpretation of results.

The seasonal variability of the airflow patterns (constructed based on the 5-day isentropic trajectories) for both NRSs – BBP and BGP – is shown in Figure 2.3.4a, and it reflects the dominance of the westerly flows in the atmospheric transport from the sites. The AHPPI boundaries (>90) for both sites intersect each other over the North Sea throughout the year, except during summer. The total area of the BBP airflow pattern is larger compared with BGP, and moreover, during spring it almost covers the BGP airflow area. During spring and fall, the BGP airflow pattern is more extended in the western direction from the site toward the North Atlantic Ocean. Throughout the year, the Faeroes Islands will be located within 25-50% of BBP AHPPI, except during winter. Considering a minimal isoline of 25% of AHPPI, it should be noted that the central parts of the Scandinavian Peninsula are less reachable throughout the year, except during spring, and hence, the NRS possible impact is lower compared with Denmark. For the Faeroes Islands, the BBP possible impact will vary between 25-55% of AHPPI, although for Iceland it is very lower than 25% of AHPPI.

The seasonal variability of the fast transport patterns (constructed at 24 hours of atmospheric transport) for both NRSs – BBP and LRS – is shown in Figure 2.3.4b. For BBP, during spring and fall the AHPPI boundaries are extended significantly to the south of the site, and moreover, during spring the three maxima of AHPPI could be identified over the Denmark, United Kingdom, and Ireland. During winter and spring, the boundaries of the fast transport probability field (enclosed by

25% of AHPPI isoline), are extended farther to north and south compared with other seasons. In general, among the Scandinavian countries only Denmark and the southern territories of Norway and Sweden could be affected by the end of the first day after an accidental release of radioactivity occurred from the site.

Airflow	*Fast Transport 24 hours*	*Fast Transport 12 hours*

(Spr)	(Spr)	(Spr)
(Sum)	(Sum)	(Sum)
(Fal)	(Fal)	(Fal)
(Win)	(Win)	(Win)
(a)	(b)	(c)

Figure 2.3.4. Seasonal variability of the: a) airflow probability fields for the blocks of the British (BBP) and German (BGP) NPPs; b) fast transport probability fields after 24 hours of atmospheric transport from the block of the British (BBP) and Loviisa (LRS) NPPs, and c) fast transport probability fields after 12 hours of atmospheric transport from the block of the British (BBP), Loviisa (LRS), and Barsebaeck (BNP) NPPs.

20

For LRS, during summer the AHPPI boundaries are more extended to the southeast of the site, during winter – to northeast of the site. Throughout the year, the total area of the fast transport probability field for LRS is smaller compared with BBP, which could be also affected by the difference in the continental vs. maritime climatical regimes of the sites, respectively. The probability of reaching the eastern seashore of Sweden is low, and the NRS possible impact there will be only 25% of AHPPI. The southern territories of Finland are always inside the LRS AHPPI boundaries throughout the year, except during summer.

The seasonal variability of the fast transport patterns (constructed at 12 hours of atmospheric transport) for three NRSs – BBP, LRS, and BNP – is shown in Figure 2.3.4c. For all NRSs, the dominating transport pattern during the first 12 hours of atmospheric transport from the sites is transport in the eastern direction. The sites' AHPPI boundaries are extended to the east of the sites, although for BBP it is extended more to the north of BBP during summer and to the west of BBP during spring, as well as for BNP it is extended to the west of BNP during fall. The seasonal variability for LRS is less pronounced, and, in general, the LRS AHPPI boundaries are located within the same geographical regions throughout the year. After 12 hours of atmospheric transport from the sites, only neighbouring to NRS countries and regions will be located within the AHPPI boundaries. For LRS, it is Finland, Estonia, and border regions of the Northwest Russia. For BNP, it is Denmark, south of Sweden, and the Baltic seashore of Germany and Poland. For BBP, it is only the United Kingdom with the western parts of the North Sea.

If consider Denmark as a country of concern than after the first 12 hours of atmospheric transport: 1) throughout the year, LRS does not affect the Danish territory 2) BNP will always represent the highest risk of atmospheric transport to Denmark throughout the year, especially during spring and fall when the AHPPI boundaries pass over the Danish borders, and 3) BBP shows the fast transport toward Denmark, and the NRS possible impact over the Danish territory will be 10-25% of AHPPI.

Finally, it should be noted that similarly to the airflow analysis we can analyse the NRS possible impact (on the concrete geographical region, territory, country, site, etc.) based the selected probabilistic fields (fast transport after 12 and 24 hours of atmospheric transport) for different time periods (annual, seasonal, and monthly variability of the fields) for any of 11 selected NRSs in the Euro-Arctic region both separately for each site or combined for several sites. For example, such FT probability fields analysis by months (during the Kursk nuclear submarine lifting and transportation operation) is given by *Mahura et al., 2002a*. The seasonal and monthly variability of the FT probability fields for the selected NRSs in the Euro-Arctic region is stored on CD (enclosed if ordered) and in Appendices 2 and 3.

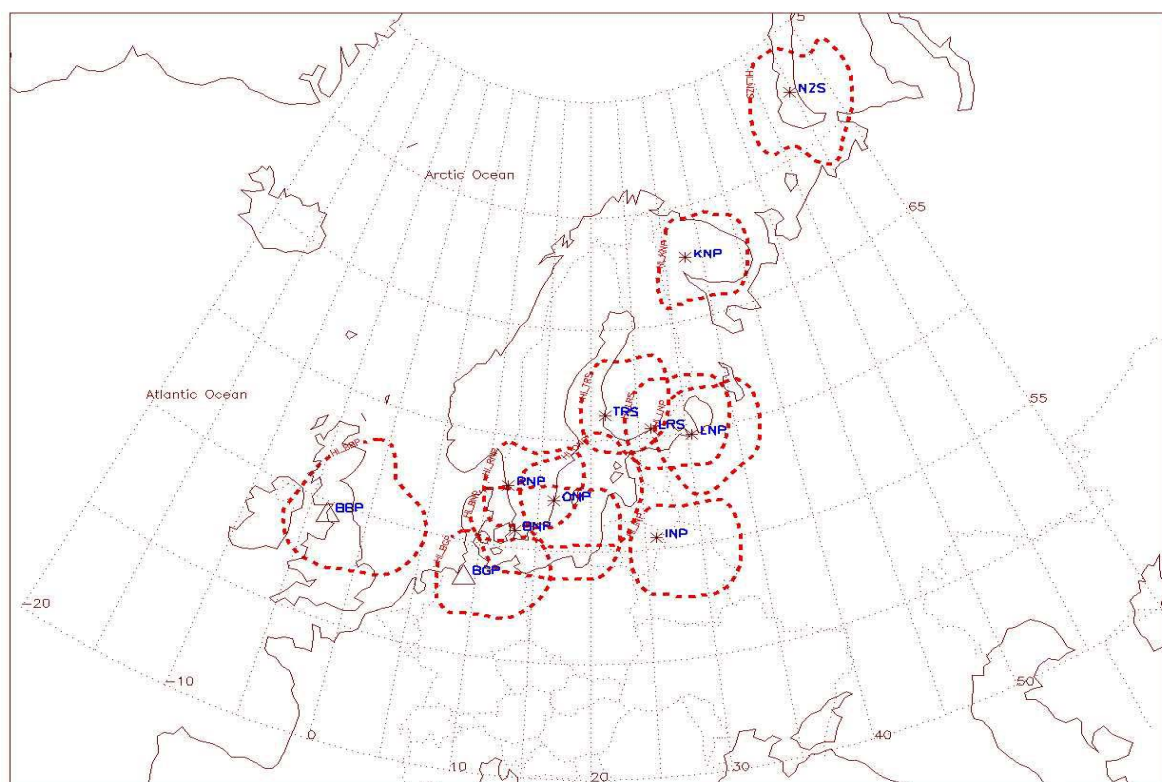## 2.4. *MAXIMUM POSSIBLE IMPACT ZONE AND MAXIMUM REACHING DISTANCE*

In this section of report, we will introduce two additional indicators (*Baklanov & Mahura, 2001; Mahura, 2001; Mahura et al., 2002a; Mahura et al., 2002d*), which could play a role of indicators of the NRS possible impact, and which, first of all, are important for the emergency preparedness. In addition to the airflow and fast transport probability fields (described in §2.2 and §2.3) it will be the **third type of probabilistic fields**. It should be noted that this type of the field, first, indicates boundaries of areas with the highest probability of being reached by trajectories during the first day of atmospheric transport from the risk sites. Let's call it **maximum possible impact zone - MPIZ**. Second, this type of the field indicates the farthest boundaries on the geographical map that might be reached during the first day by, at least, one trajectory originating over the NRS location. Let's call it **maximum reaching distance - MRD**.

To visualise the MPIZ indicator we counted also all endpoints of calculated trajectories originated within the boundary layer (such calculation can be done for any other layer or altitude) during the first day of transport (at 12 and 24 hours). Then, a similar approach for construction of probability fields (as was used for the airflow and fast transport probability fields; see §2.2) was used to construct the MPIZ field. An isoline of MPIZ was drawn through the areas with the highest occurrence of trajectory intersections with the cells of the gridded domain.

To visualise the MRD indicator we used all endpoints of calculated trajectories at the end of the first day of atmospheric transport. An isoline of MRD was drawn through the grid cells where, at least, one trajectory intersected with the grid cell boundaries. We should note also, that although the likelihood that an air parcel will reach these boundaries is low, it is still a possible case of atmospheric transport from the site.

Maximum Possible Impact Zone

Maximum possible impact zone (MPIZ) indicator, similarly to the fast transport probability fields, is important characteristic of the NRS possible impact during the first day of atmospheric transport after an accidental release at the site. The boundaries of the MPIZ indicators for the selected NRSs in the Euro-Arctic region are shown in Figure 2.4.1. It should be noted, that although MPIZs are concentrated in a vicinity of the risk sites, the configuration of the MPIZ isolines will depend on the dominating transport patterns during the first day of atmospheric transport, and isolines are extended along the direction of the main flow. For majority of the selected NRSs, the dominating airflows from the sites are westerlies. Additionally, for the BBP site the MPIZ boundaries are extended to the north of BBP. For the NZS, KNP, LNP, and INP sites these boundaries are extended to the south of the sites.

Figure 2.4.1. Annual boundaries of the maximum possible impact zone indicators after 24 hours of atmospheric transport for the selected NRSs in the Euro-Arctic region.

For studies of the long-term consequences of routine discharges or accidental releases it is important to evaluate not only boundaries of MPIZ, but also areas of regions enclosed by the MPIZ boundaries. To estimate areas we used a simple approach. First, the figure inside the MPIZ boundary (or isoline) was approximated by a set of triangles, where each triangle has a top at the NRS coordinates and a side on the MPIZ isoline. Second, the areas of all triangles were calculated, and the total area under the MPIZ isoline was equal to a sum of all triangles' areas. The estimation of monthly maximum, minimum, and average areas for MPIZ is given in Table 2.4.1. It should be noted that areas' variability depends on the wind velocities on the synoptic- and mesoscales throughout the year. And although, in general, during winter the wind speeds are higher compared with summer, there is a possibility in variability defined by the local-scale atmospheric processes.

Table 2.4.1. Monthly variability of the maximum possible impact zone indicator.

Nuclear Risk Sites	NRS	Area of MPIZ $\cdot 10^4$ km^2		
		Maximum	*Minimum*	*Annual Average*
Novaya Zemlya Test Site	NZS	91.5 (Dec)	42.9 (May)	57.4
Kola NPP	KNP	52.4 (Apr)	31.9 (Aug)	42.8
Leningrad NPP	LNP	52.4 (Nov)	30.9 (Sep)	40.2
Ignalina NPP	INP	56.0 (Feb)	35.2 (Nov)	42.0
Oskarshamn NPP	ONP	66.5 (Mar)	29.0 (Aug)	41.8
Ringhals NPP	RNP	50.7 (Apr)	28.3 (Aug)	38.3
Barsebaeck NPP	BNP	61.3 (Mar)	28.5 (Jun)	40.2
Loviisa NPP	LRS	51.4 (Jul)	29.5 (Oct)	40.9
Olkiluoto (TVO) NPP	TRS	55.9 (Nov)	33.8 (May)	44.6
Block of the British NPPs	BBP	61.2 (Apr)	29.9 (Jul)	43.7
Block of the German NPPs	BGP	63.6 (Nov)	28.9 (Jun)	42.1

**Table 2.4.2.** Seasonal variability of the maximum possible impact zone indicator.

Nuclear Risk Sites	NRS	Area of MPIZ $\cdot 10^4$ km^2	
		Maximum	*Minimum*
Novaya Zemlya Test Site	NZS	79.7 (Win)	47.1 (Sum)
Kola NPP	KNP	41.9 (Spr)	33.6 (Sum)
Leningrad NPP	LNP	57.4 (Win)	34.4 (Fal)
Ignalina NPP	INP	56.9 (Win)	32.1 (Fal)
Oskarshamn NPP	ONP	62.3 (Win)	37.7 (Sum)
Ringhals NPP	RNP	46.0 (Spr)	27.9 (Sum)
Barsebaeck NPP	BNP	44.9 (Win)	35.8 (Fal)
Loviisa NPP	LRS	43.8 (Fal)	31.4 (Sum)
Olkiluoto (TVO) NPP	TRS	48.1 (Fal)	33.9 (Spr)
Block of the British NPPs	BBP	66.8 (Spr)	32.1 (Sum)
Block of the German NPPs	BGP	45.6 (Win)	30.3 (Sum)

If consider a standard division by seasons (where: Win=Dec+Jan+Feb, Spr=Mar+Apr+May, Sum=Jun+Jul+Aug, and Fal=Sep+Oct+Nov), than there is a possibility of significant smoothing in the monthly fields and MPIZ areas, and therefore, shifting of extremes. On a seasonal scale (Table 2.4.2), for more than half of NRSs the MPIZ area has a minimum in summer, except Leningrad (LNP), Ignalina (INP), and Barsebaeck (BNP) NPPs, where it has a minimum in fall. Moreover, the monthly minimum (Table 2.4.1) or maximum could be shifted by 1-2 months with respect to seasonal extremes (Table 2.4.2). For example, for the Leningrad NPP (LNP), the monthly

maximum is in November, but seasonal maximum is in winter; for the Novaya Zemlya Test Site (NZS), the monthly minimum is in May, but seasonal minimum is in summer; etc. It should be noted that for NZS, the MPIZ area - $91.5 \cdot 10^4$ km^2 - is maximal among 11 considered nuclear risk sites.
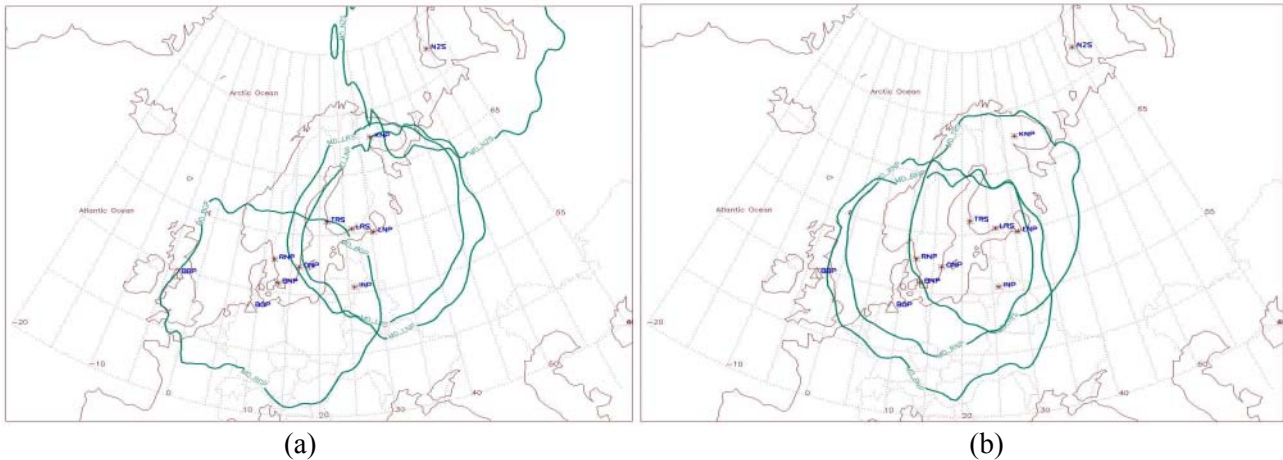
Maximum Reaching Distance

Maximum reaching distance (MRD) indicator, similarly to the maximum possible impact zone indicator, is important characteristic of the NRS possible impact during the first day of atmospheric transport after an accidental release at the site. The boundaries of the MRD indicators for the selected NRSs in the Euro-Arctic region are shown in Figures 2.4.2 and Figure 2.4.3. If consider a large dataset of trajectories, there is a situation after the hypothetical accidental release when the contaminated air parcels might reach the most remote geographical regions. The distance to these remote boundaries might vary between hundreds and thousands kilometres. Boundaries, depicted on Figures 2.4.2 and 2.4.3 reflect such possibility. They could be interpreted as probable boundaries of the NRS possible impact during the first day after the hypothetical accidental release when atmospheric transport from the site was the fastest.
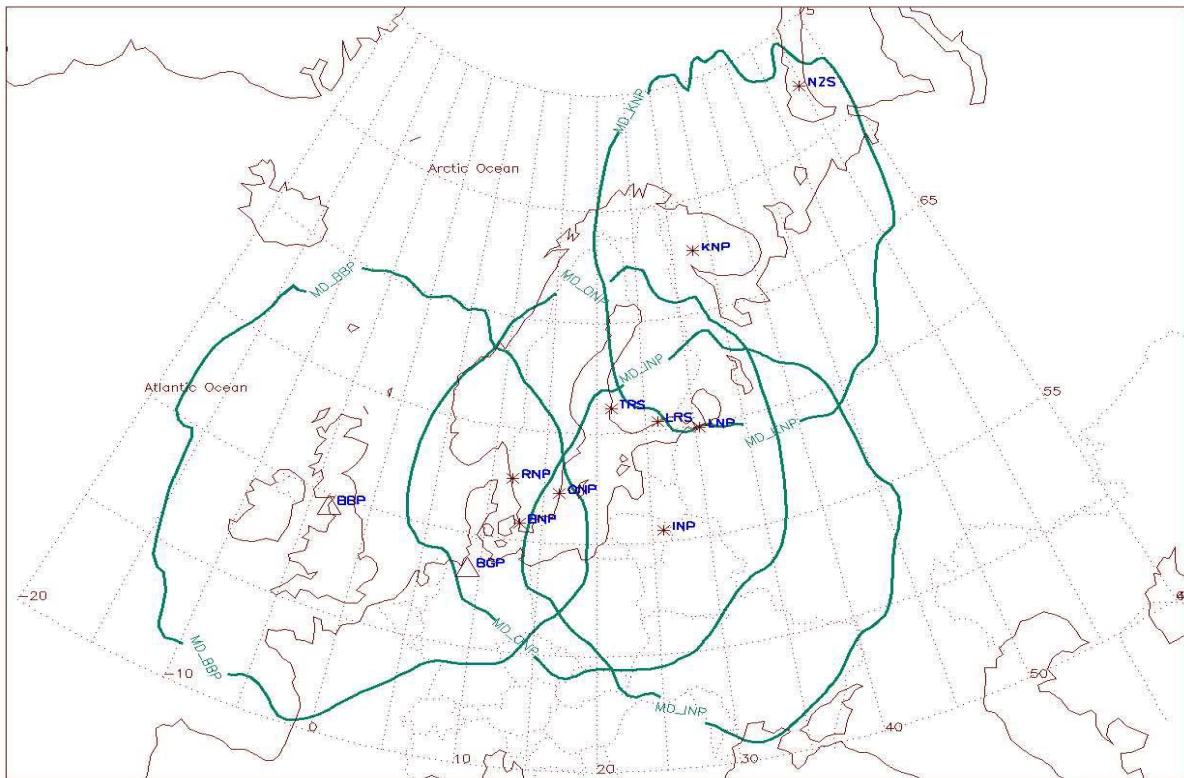
Figure 2.4.2. Annual boundaries of the maximum reaching distance indicator after 24 hours of atmospheric transport for the Block of the British NPPs (MD_BBP), Oskarshamn NPP (MD_ONP), Ignalina NPP (MD_INP), and Kola NPP (MD_KNP).

For example, for the Kola NPP (KNP), the zone of such impact is extended to the northern territories of Sweden and Norway, most of the territory of Finland, and north-western territories of Russia (including the Barents, White, and Kara Seas) (Figure 2.4.2). For the Leningrad NPP (LNP), the boundaries include a significant part of Finland, Baltic States, Byelorussia, northwest and central regions of Russia (Figure 2.4.3a). For the Novaya Zemlya Test Site (NZS), the atmospheric transport is extended in the latitudinal direction by 20-30° from the site, and in the meridional direction – 8-10° from the site (Figure 2.4.3a). For the Olkiluoto (or TVO) NPP (TRS), the MRD

boundaries are extended over the large part of the Scandinavian Peninsula, Northwest Russia, Baltic States, and, partially, over Byelorussia and Poland (Figure 2.4.3b).


| (a) | (b) |

Figure 2.4.3. Annual boundaries of the maximum reaching distance indicator after 24 hours of atmospheric transport for the: a) Block of the German NPPs (MD_BGP), Loviisa NPP (MD_LRS), Novaya Zemlya Test Site (MD_NZS), and Leningrad NPP (MD_LNP); and b) Barsebaeck NPP (MD_BNP), Ringhals NPP (MD_RNP), and Olkiluoto NPP (MD_TRS).

Additionally, similarly to MPIZ, it is possible to estimate an area enclosed by the MRD isolines for each NRS (Table 2.4.3). The MRD areas, of course, are significantly large than the MPIZ areas, and the latter is also included in the MRD area. But in comparison with MPIZ, the dominating direction of atmospheric transport is less underlined by MRD. The MRD areas have also temporal: seasonal (Table 2.4.3) and monthly variability. Because the construction of the MRD indicator boundaries includes cells of gridded domain with the lowest probabilities of transport through the cells (i.e. at least one trajectory reached a cell), it is not possible to explain such variability only by the synoptical scale features (i.e. there is a contribution of the global scale patterns, as well as anomalies in the general transport patterns from the sites throughout the year). Among 11 NRSs there are two: one with the highest and one with the lowest MRD areas. For the Novaya Zemlya Test Site (NZS), the annual MRD area is equal to $903.5 \cdot 10^4$ km^2 with a maximum during winter, and for the Oskarshamn NPP (ONP), it is equal to $595.1 \cdot 10^4$ km^2 with a minimum during spring.

Table 2.4.3. Seasonal variability of the maximum reaching distance indicator.

Nuclear Risk Sites	NRS	Area of MRD $\cdot 10^4$ km^2		
		Maximum	*Minimum*	*Annual Average*
Novaya Zemlya Test Site	NZS	1200.0 (Win)	361.4 (Sum)	903.5
Kola NPP	KNP	975.2 (Spr)	427.1 (Win)	596.0
Leningrad NPP	LNP	785.5 (Win)	330.9 (Fal)	691.6
Ignalina NPP	INP	842.7 (Win)	540.0 (Sum)	703.0
Oskarshamn NPP	ONP	1007.4 (Win)	457.1 (Spr)	595.1
Ringhals NPP	RNP	1307.2 (Win)	618.1 (Fal)	854.5
Barsebaeck NPP	BNP	1296.3 (Win)	547.9 (Fal)	815.6
Loviisa NPP	LRS	1039.3 (Win)	475.9 (Sum)	810.3
Olkiluoto (TVO) NPP	TRS	1160.4 (Win)	647.9 (Sum)	780.9
Block of the British NPPs	BBP	1100.0 (Win)	385.9 (Spr)	817.0
Block of the German NPPs	BGP	962.4 (Spr)	568.6 (Sum)	735.6

Block of the British NPPs	***Barsebaeck NPP***	***Kola NPP***

(Spr)	(Spr)	(Spr)
(Sum)	(Sum)	(Sum)
(Fal)	(Fal)	(Fal)
(Win)	(Win)	(Win)
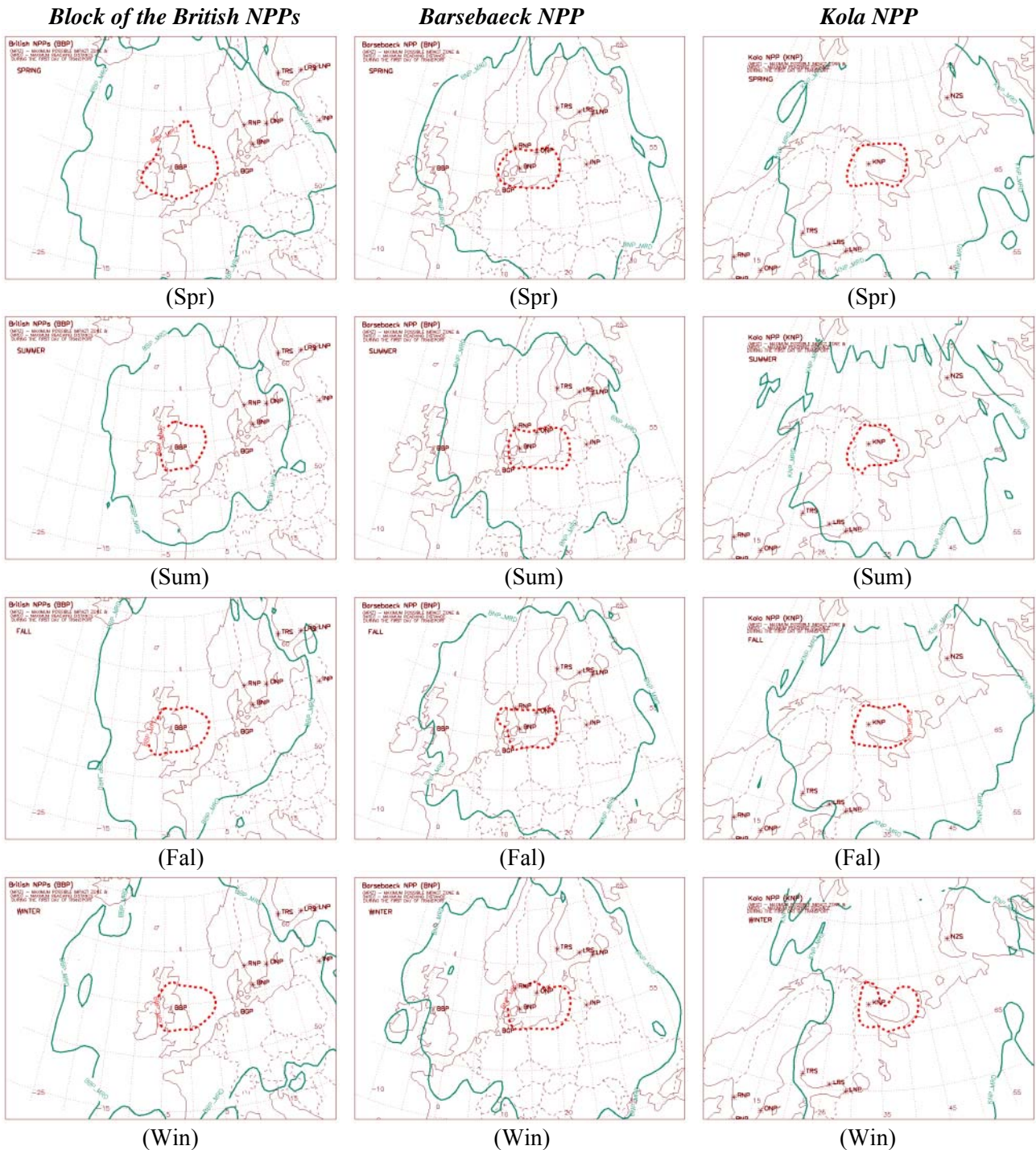
Figure 2.4.4. Seasonal variability of the maximum reaching distance and maximum possible impact zone for the Block of the British NPPs – BBP (left), Barsebaeck NPP – BNP (middle), and Kola NPP – KNP (right).

Several examples with the seasonal variability of the MPIZ and MRD indicators combined into one figure are shown in Figure 2.4.4 for the block of the British (BBP), Barsebaeck (BNP), and Kola (KNP) NPPs. Plotting of both indicators simultaneously allows to estimate the order of difference between impacted areas and farthest indicator's boundaries, and between the highest (MPIZ) and the lowest (MRD) probabilities of the NRS possible impact on the geographical territories. The annual (Figure 2.4.5), monthly (Appendix 4), and seasonal variability of both indicators for 11 selected NRSs in the Euro-Arctic region is stored on CD (enclosed if ordered).
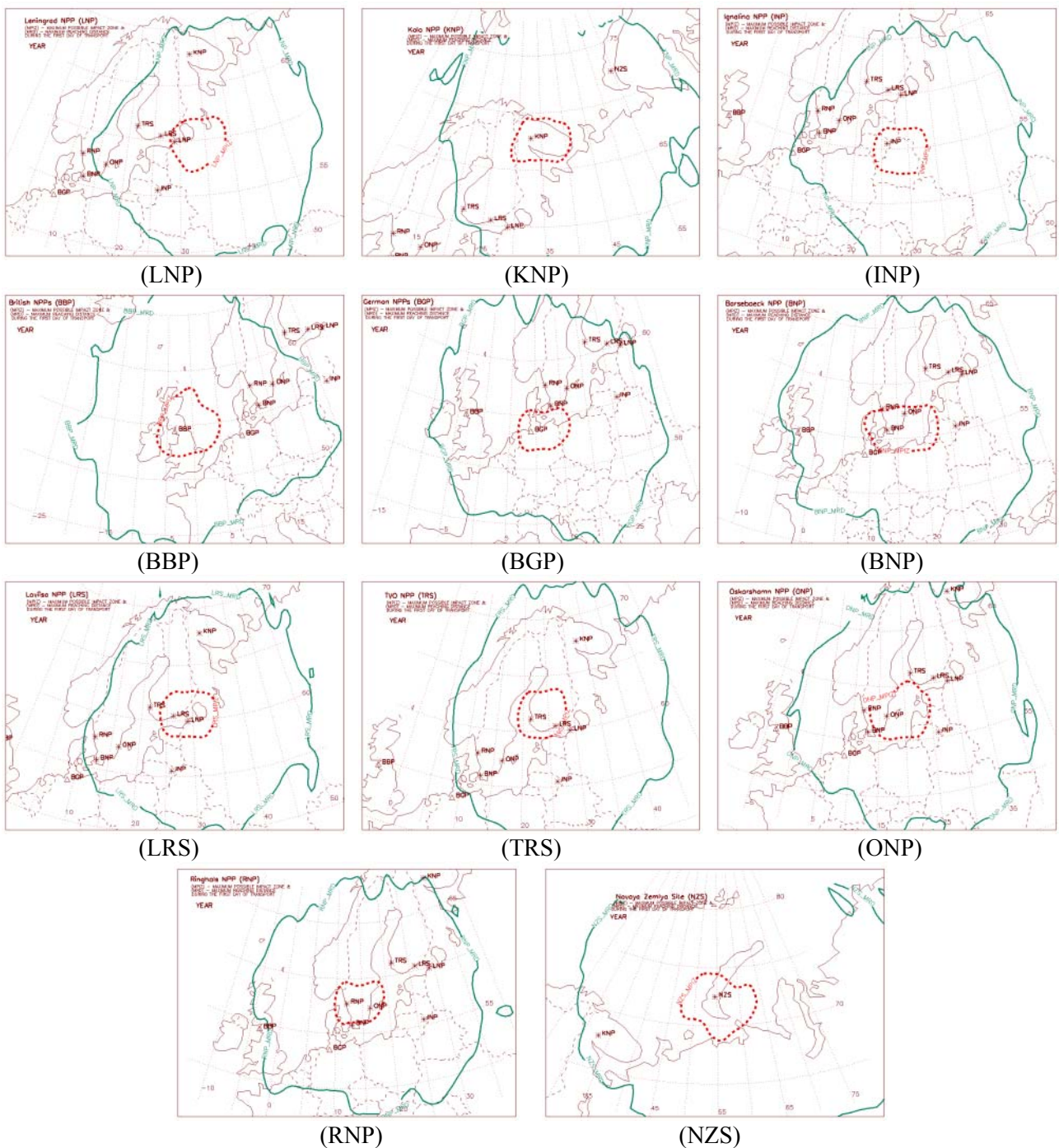
(LNP)	(KNP)	(INP)
(BBP)	(BGP)	(BNP)
(LRS)	(TRS)	(ONP)
(RNP)	(NZS)	

Figure 2.4.5. Annual maximum reaching distance and maximum possible impact zone for the selected NRSs in the Euro-Arctic region.

2.5. *TYPICAL TRANSPORT TIME FIELDS*

In the emergency response systems for nuclear accidents, the estimation of the radionuclide transport time to a particular territory, region, county, city, etc. is one of the important input parameters in the decision-making process. We extracted this information from the calculated isentropic trajectories and constructed the **<u>fourth type of probabilistic fields</u>** called the **typical transport time (TTT) fields**. These fields show: first, how long it will take for an air parcel to

reach a particular geographical area from the NRS location, and second, what areas would be at the highest risk during the first few days of radionuclide cloud transport after an accident at NRS.

__Construction of Typical Transport Time Fields__

To construct the TTT fields, at the first step, we built a new polar grid domain having 36 sectors (10° each) and 35 grid cells (2° each) along each sector line with the risk site in the center. At the second step, in the same way as in the probability fields analysis, we counted the number of trajectory intersections in each grid cell of new domain. Then, we selected along each sector a grid cell with absolute maximum of trajectory intersections and constructed an isoline of typical transport time.

A similar procedure is repeated for each temporal term of 0.5, 1, 1.5, 2, and 2.5 days. As a step of this procedure, initially, the geographical coordinates (latitude and longitude) were converted into polar coordinates (radius $R(X_t, Y_t)$ and polar angle $\alpha(X_t, Y_t)$):

$$R(X_t, Y_t) = \sqrt{\left(X_t - X_{NRS}\right)^2 + \left(Y_t - Y_{NRS}\right)^2},$$

$$\gamma(X_t, Y_t) = \arctan\left(\frac{\left(Y_t - Y_{NRS}\right)}{\left(X_t - X_{NRS}\right)}\right),$$

$$\alpha(X_t, Y_t) = \begin{cases} 90 - \gamma(X_t, Y_t) & \text{if} \quad N - E \\ 90 + \gamma(X_t, Y_t) & \text{if} \quad E - S \\ 180 + \gamma(X_t, Y_t) & \text{if} \quad S - W \\ 270 + \gamma(X_t, Y_t) & \text{if} \quad W - N \end{cases},$$

where:

X_t, Y_t – longitude and latitude of trajectory at time t ($t = 0{,}10$ days; $\Delta t = 12$ hours),

X_{NRS}, Y_{NRS} – longitude and latitude of the NRS location,

$\gamma(X_t, Y_t)$ – angle calculated for one of quadrants (I-IV).

Then, for each time t in each cell of the sector, we counted number of trajectory intersections $N_{CELL_{ij}}(t)$, and compared with the cells along the sector line to find a cell with the absolute maximum of trajectory intersections $N_{AMC}(t)$:

$$N_{CELL_{ij}}(t) = \sum_{j=1}^{M_{sect}} \sum_{i=1}^{M_{int}} n_{ij},$$

$$n_{ij} = \begin{cases} 0 \\ 1 \end{cases} if \quad \begin{cases} R_{grid_{i,j}} \le R(X_t, Y_t) < R_{grid_{i+1,j+1}} \\ \alpha_{grid_{i,j}} \le \alpha(X_t, Y_t) < \alpha_{grid_{i+1,j+1}} \end{cases},$$

$$N_{AMC}(t) = \max\left(N_{CELL_{1,1}}(t), ..., N_{CELL_{M_{sect}, M_{int}}}(t)\right),$$

where:

R_{grid}, α_{grid} - radius and angle of grid points in the gridded domain;

M_{sect}, M_{int} - total number of grid points of the gridded domain (36 sectors x 10° and 35+1+35=71 intervals x 2°, respectively).

For simplicity, if several AMC cells were identified along the sector line than the closest to the site was selected for construction of the TTT field (example is shown for the Leningrad NPP by *Baklanov & Mahura, 2001; Mahura, 2001*). It should be noted that the TTT fields' construction for the later terms is complicated due to significant airflow propagation from the site locations, and hence, the later terms isolines are not concentrated around the site and less representative.

Typical Transport Time Fields for NRSs in the Euro-Arctic Region

The annual typical transport time fields for a combined consideration of the NRS possible impact are shown in Figure 2.5.1, and separately for each NRS, selected in this study, are shown in Figure 2.5.2. The seasonal variability of the TTT fields is stored on CD (enclosed if ordered).

For the Block of the British NPPs (BBP), the typical situation during the first day would be atmospheric transport over the United Kingdom territories and adjacent seas without reaching the populated territories of the continental European countries (Figure 2.5.1a). After 2 days, the air mass might reach the southern territories of Norway and Sweden, as well as countries on the seashore of the North and Baltic Seas. The atmospheric transport in the southern and south-eastern directions is minimal. For the Kola NPP (KNP), during the first day the territories of the Murmansk and Archangelsk Regions, north of Karelia, and Finland could be reached, and on the second day, the large territory of the Northwest Russia, northern and central regions of the Scandinavian Peninsula are reached (Figure 2.5.1b). Moreover, a significant shift of the TTT isolines at 2 days is seen in the eastern direction (dominating airflow pattern for the KNP site).
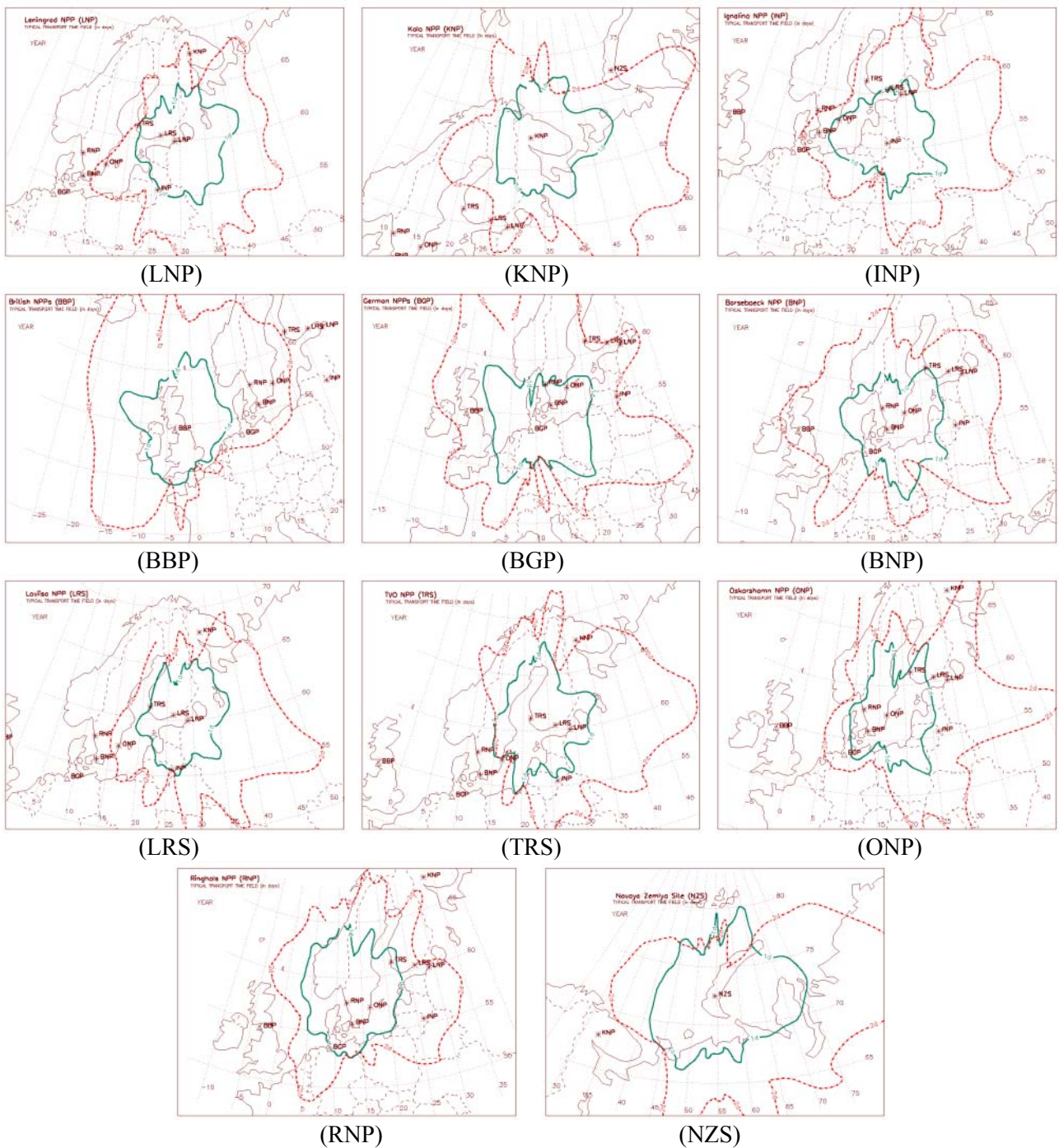

| (a) | (b) |
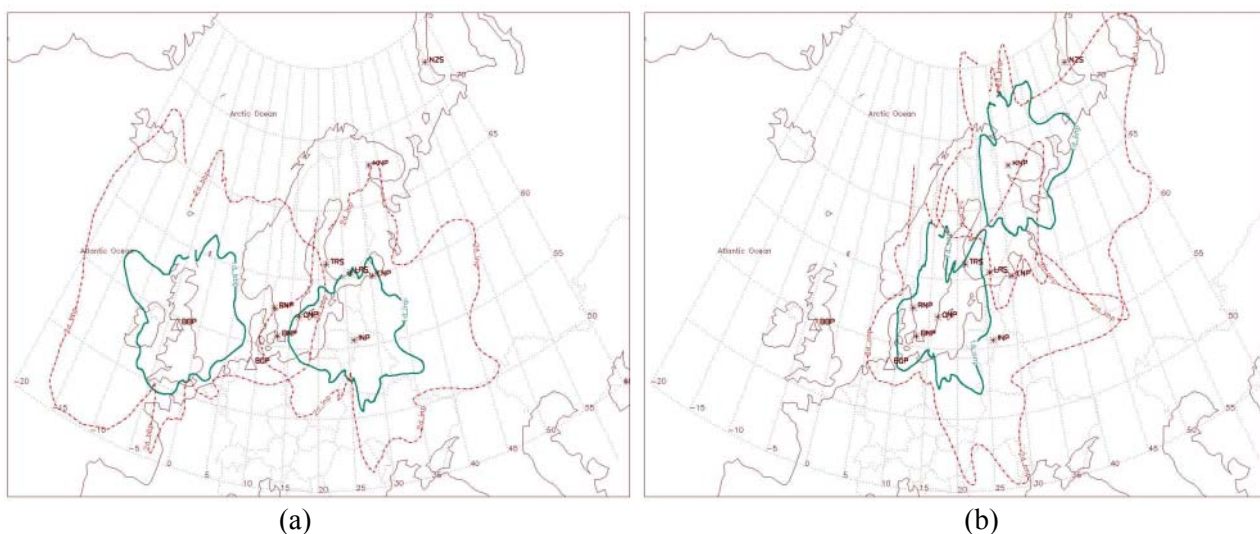
Figure 2.5.1. Annual typical transport time fields at 1 (——) and 2 (---) days of atmospheric transport for the: a) Block of the British (BBP) and Ignalina (INP) NPPs, and b) Oskarshamn (ONP) and Kola (KNP) NPPs.

If we assume, that the nuclear weapons testing would be resumed on the Novaya Zemlya Test Site (NZS) (considering possible vent emissions during underground testing as a possible source of radioactivity), than the typical transport time field shows that, on average, during the first day the contaminated air parcels will reach only the Russian Arctic seashore (Figure 2.5.2). During first two days the boundaries are extended significantly in both eastern and southern directions reaching 60°N, although countries of the Scandinavian Peninsula and Northern Europe will remain un-affected.

Detailed analysis of the TTT fields for individual and several combined NRSs allows to identify geographical regions and territories of the neighbouring countries which could be reached by atmospheric flows and might be impacted by radioactive pollution during a selected period of time, if an accidental release (or releases) occurred at NRSs. This information could be used to

forecast the arrival of the radioactive cloud to a concrete territory, and hence, it will allow to plan countermeasures, including informing and evacuating of population.

It should be also noted that selection of terms - 0.5, …, 2.5 days – depends on the used for modelling the temporal (interval of 12 hours) and horizontal (2.5° x 2.5° latitude vs. longitude) resolution of meteorological data. Although, the linear interpolation of the TTT fields could be done for the smaller time intervals (for example: 1, 3, 6, etc. hours) it will more reasonable to use a finer resolution meteorological data for modelling purposes.


(LNP)	(KNP)	(INP)
(BBP)	(BGP)	(BNP)
(LRS)	(TRS)	(ONP)
(RNP)	(NZS)	

Figure 2.5.2. Annual typical transport time fields at 1 (──) and 2 (---) days of atmospheric transport for the selected NRSs in the Euro-Arctic region.

2.6. INDICATORS OF POLLUTION POSSIBLE REMOVAL: RELATIVE HUMIDITY, PRECIPITATION, AND WET DEPOSITION FIELDS

During the atmospheric transport of any kind of pollutants, including radionuclides, many different processes may influence the distribution of substances. In general, the temporal change of the radionuclide concentration during atmospheric transport will depend on the following factors. First, the horizontal and vertical dispersion due to horizontal advection by a wind velocity vector and turbulent diffusion are the most important factors. Second, all radionuclides during atmospheric transport are subject to dry deposition of gaseous and particulate nuclides from the atmosphere by vegetation, biological, or mechanical processes as well as to wet removal by precipitation: rain and snow. Third, other factors are radioactive decay and resuspension (i.e. lifting of already deposited material again back into the atmosphere). Although the contributions of all factors are important, there is always a possibility to ignore some of them depending on the scale of analysis and each term's contribution to a particular problem. There are several approaches, which may be used to evaluate possible contributions to radionuclide removal during atmospheric transport. Let us consider them in more details in this section of report.

The **first approach** is based on **evaluation of the long-term climatological patterns** for relative humidity and precipitation for a particular geographical area or region of interest. Such climatological maps (on a multiyear, seasonal, or monthly basis for the large scale domains) can be obtained from the meteorological weather services or constructed from the climatological data archives. These maps would reflect the accumulated precipitation or relative humidity measured near the surface for each interval of time. It can be used for identification of the large areas having common precipitation and relative humidity patterns. For example, NOAA-CIRES Climate Diagnostic Center (CDC) (http://www.cdc.noaa.gov) allows, based on their data archives, to construct the **averaged climatological relative humidity fields** for different temporal intervals – multiyear (Figure 2.6.1), months and seasons (Figure 2.6.2). Similarly, it is possible to construct the **averaged climatological precipitation fields** for various temporal intervals as shown in Figure 2.6.3 (for a multiyear period), and Figure 2.6.4 (for selected month and season).

(a)   (b)
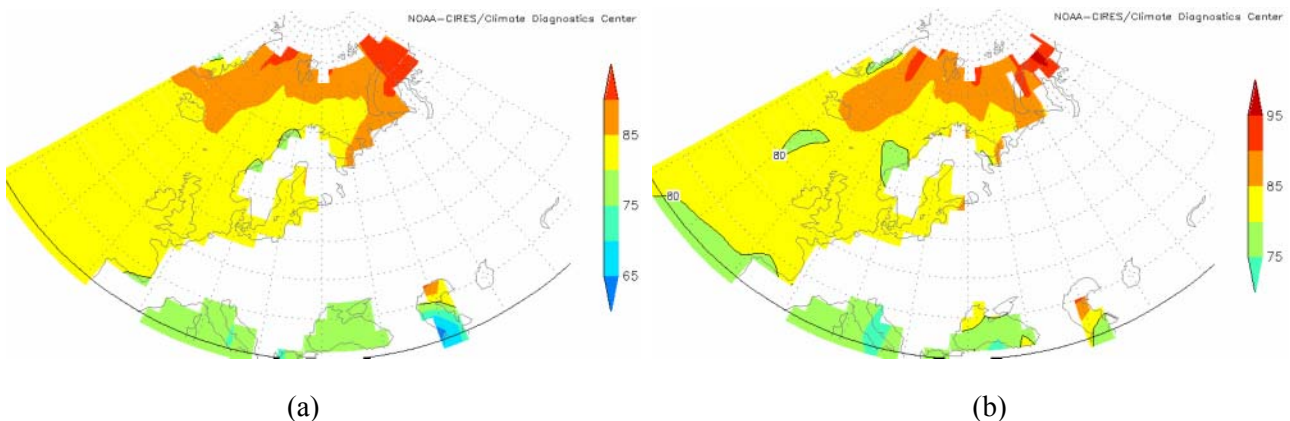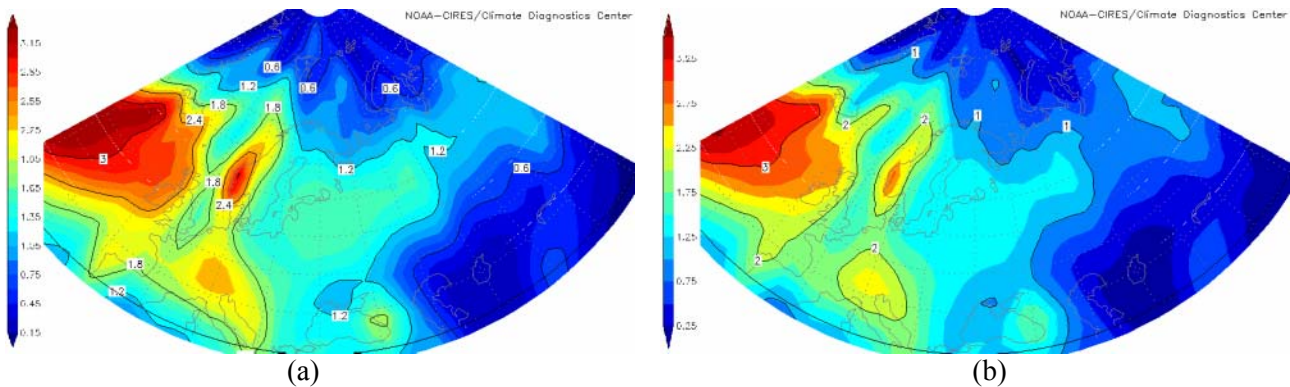
Figure 2.6.1. Mean relative humidity (%) fields for the Northern Europe and adjacent regions based on a) Jan 1800 – Dec 1997 and b) Jan 1991 – Dec 1996 data (*Source: NOAA-CIRES CDC*).

The **second approach** is based on **evaluation** of the probabilistic fields for the "precipitation factor" **based on trajectory modelling results** (*Mahura et al., 1999a; INTAS, 2000; Mahura et al., 2001; Mahura, 2001*). There the relative humidity "plays the role" of a precipitation factor. It is one of the factors, which will roughly determine the possibility of radionuclide removal during atmospheric transport. Increasing relative humidity in the atmosphere is one of the signals of the

water vapor's increasing presence, and it may, in the presence of the cloud condensation nuclei (CCN), lead to the formation of cloud cover. After clouds develop and form, under certain conditions there is a possibility of precipitation, and hence, radionuclide removal. Construction of the relative humidity fields is similar to the first steps in the probability field analysis. In this case we calculate an average value of the relative humidity in each grid cell.

(a)   (b)
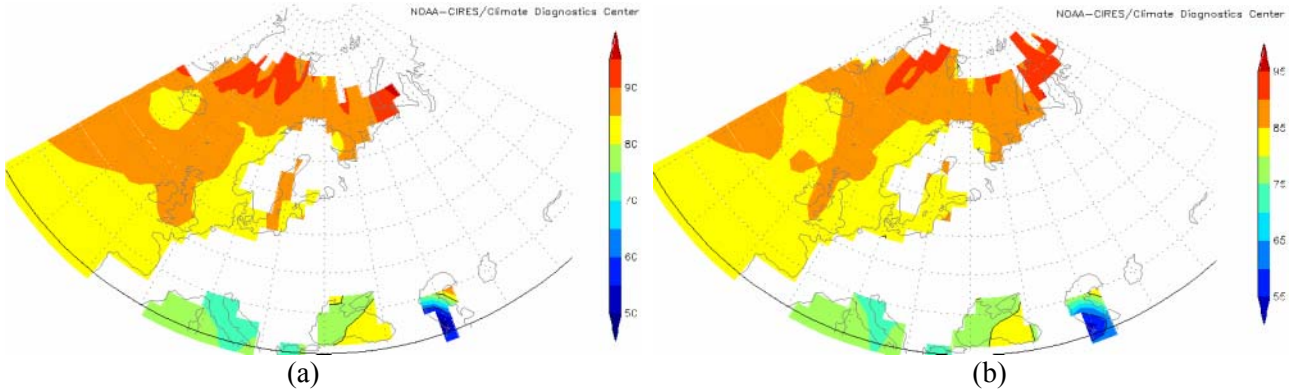
Figure 2.6.2. Long-term mean relative humidity (%) fields for the Northern Europe and adjacent regions for a) July and b) Summer (*Source: NOAA-CIRES CDC*).


(a)   (b)

Figure 2.6.3. Mean precipitation (mm/day) fields for the Northern Europe and adjacent regions based on a) Jan 1979 – Dec 1999 and b) Jan 1991 – Dec 1996 data (*Source: NOAA-CIRES CDC*).


(a)   (b)
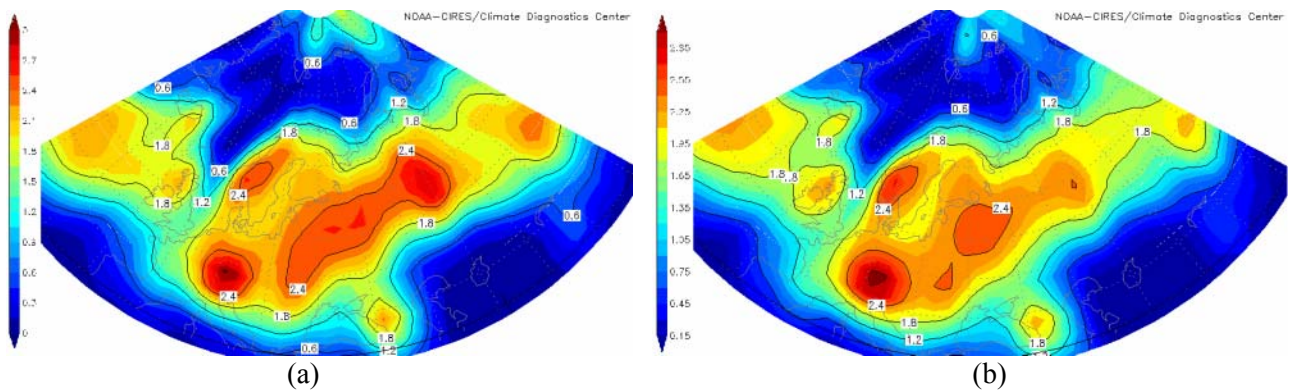
Figure 2.6.4. Long-term mean precipitation (mm/day) fields for the Northern Europe and adjacent regions for a) July and b) Summer (*Source: NOAA-CIRES CDC*).

Both the precipitation and relative humidity fields have a cellular structure in comparison with the airflow pattern. A pitfall in this analysis is the fact that all relative humidity values are directly

related to the existing flow pattern from the site. So, each field is valid only with respect to a particular NRS. Nevertheless, it is more realistic pattern of the possible removal during transport than calculating climatological maps used in the first approach, because it includes processes above the surface.

| (a) | (b) | (c) |
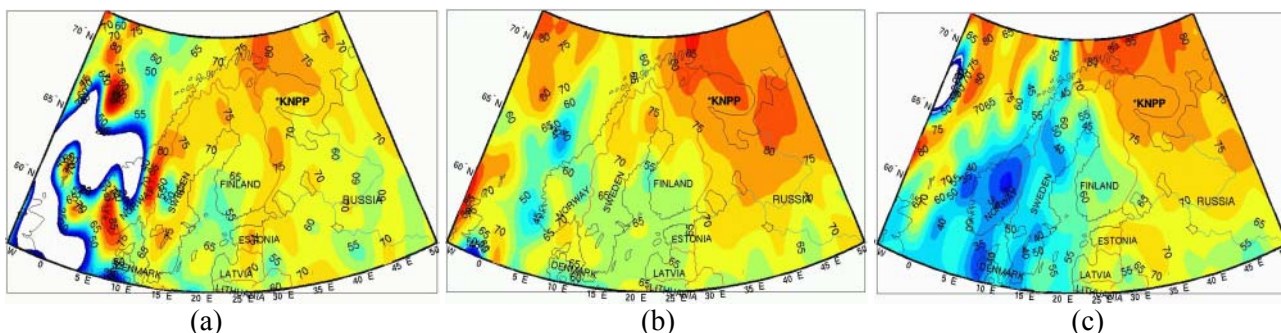
Figure 2.6.5. Relative humidity (or precipitation factor) fields for the Kola NPP within the boundary layer: a) summer, b) fall, and c) winter.

| (a) | (b) |
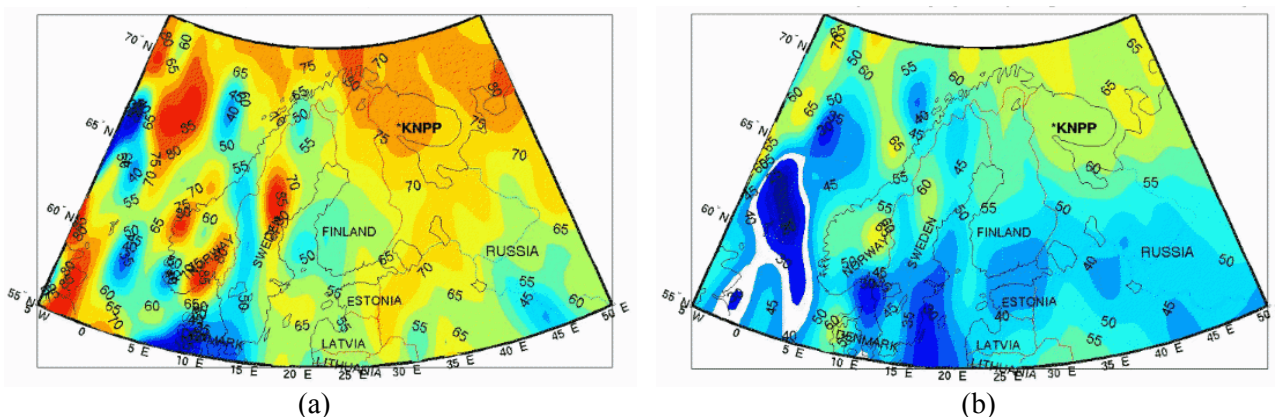
Figure 2.6.6. Spring relative humidity (or precipitation factor) fields for the Kola NPP in the layer of a) surface – 1.5 km asl and b) 1.5-3 km asl.

This type of the fields - **relative humidity or precipitation factor fields** - describes the possibility for removal processes to impact the contaminated air mass as it passes over the particular geographical area. Such an analysis, a simple approximation, was used in *INTAS, 2000; OCB, 2000; CERUM, 2001* and *AR-NARP, 2001-2003* studies. To account for the contribution of radionuclide wet removal during atmospheric transport, the temporal and spatial distribution of relative humidity was calculated by constructing the relative humidity fields over the geographical areas of concern. Seasonal variability of the relative humidity fields within the boundary layer (for simplification it is assumed to be: surface - 1.5 km asl) for the trajectories originating over the Kola NPP region during 1991-1996 is shown in Figure 2.6.5 and 2.6.6a. In some cases, for example Figure 2.6.5a, the trajectories did not reach some geographical territories (shown as an "empty spot" in the left bottom corner of the figure) during summer; therefore, the relative humidity over this region was not calculated.

Additionally, several atmospheric layers - surface - 1.5, 1.5-3, 3-5, and above 5 km asl - were examined to determine altitudinal differences in the possible removal processes (see examples in Figure 2.6.6). As a first approximation, it was assumed that areas with relative humidity above 65% were areas, where water vapor could be condensed and later removed in the form of precipitation. The limitation of this approach is how we might resolve precipitation processes during air parcels transport (for example, to resolve it we might need a finer meteorological data resolution). Analysis

of relative humidity fields for the Kola NPP showed that the precipitation factor's contribution dominates in the low troposphere layers, and areas associated with the Icelandic Low activity and along the main tracks of the cyclone systems.

The **third approach** is based on **direct evaluation** of the wet deposition fields (as the precipitation factor field) **based on dispersion modelling results** (*AR-NARP, 2001-2003; Baklanov et al., 2002; Baklanov et al., 2002*). For this purpose, we can run a dispersion model for a multiyear period and include one of the parameters of interest. As input data for such run we could use meteorological data including precipitation from the: 1) National Center for Environmental Prediction (NCEP, USA, North America), 2) European Center Medium Weather Forecast (ECMWF, Reiding, United Kingdom, Europe), or 3) DMI-HIRLAM model with a high resolution data up to 0.15º x 0.15º latitude vs. longitude.

In this approach, assuming a continuous **u**nit (for example, for a day, month, season, or year) **d**iscrete (for example, every selected time interval of 15 minutes, 60 minutes, 3 hours, etc.) **h**ypothetical **r**elease (UDHR) of puffs occurred at NRS, we can run a model of atmospheric transport, dispersion, and deposition (both dry and wet) of the radioactive material. As a result of such simulation, we can produce a field for the wet deposition patterns (see examples in Figure 2.6.7) accumulated or averaged during selected time period (for example, day, month, season, year, or multiyear period). Analysis of such field allows one to estimate: what would be accumulated wet deposition patterns if a continuous release of radioactivity took place at NRS. Moreover, analysis of such field also allows identification of the geographical areas (presumably of the cellular nature) where the precipitation is observed. These areas are territories where the greatest removal of radionuclides is possible during atmospheric transport from NRS. It should be noted that such fields are also valid (as in the second approach mentioned) with respect to a particular NRS of interest and they are related to trajectories representing atmospheric transport.

| (a) | (b) |
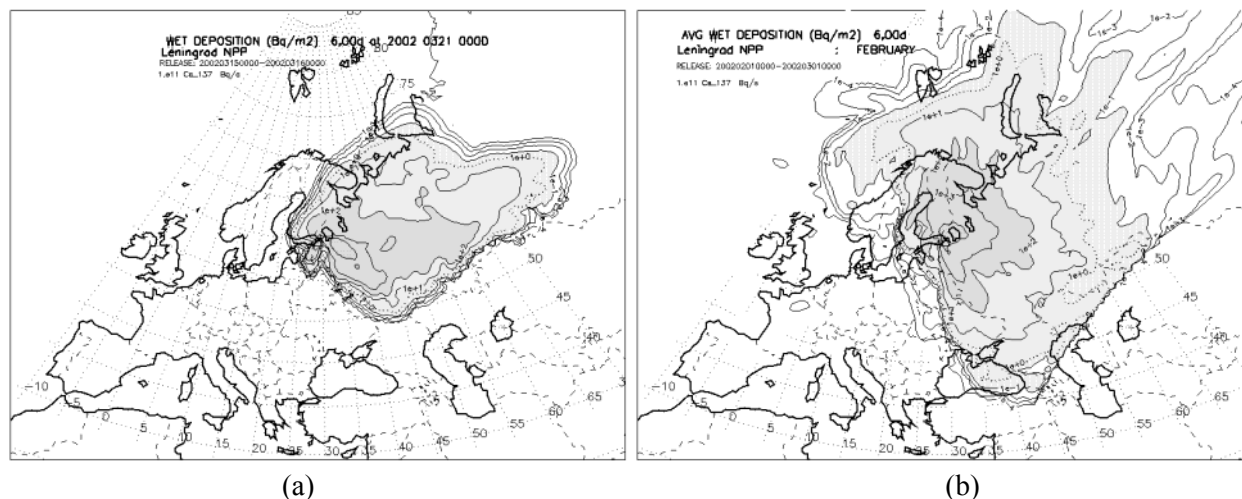
Figure 2.6.7. ^{137}Cs wet deposition fields for the unit discrete hypothetical release at the Kola NPP during a) 15-16 Mar 2002, 00 UTC, and b) 1 Feb – 1 Mar 2002, 00 UTC.

The methodological aspects of the dispersion modeling approach to calculate the wet deposition fields and their statistical characteristics are discussed by *Baklanov et al., 2002*, and results of modeling and wet deposition fields analysis for the selected NRSs in the Euro-Arctic region will be presented by *Mahura et al., 2003*.

CONCLUSION

The main aim of this study is 1) to test a methodology for evaluation of the atmospheric transport of radioactive pollutants from the nuclear risk sites to different geographical regions and countries, and 2) to combine atmospheric transport modeling and statistical analyses to evaluate possible impact of an accidental release at the nuclear risk sites located at the Euro-Arctic region. The main purpose of this study is a probabilistic analysis of atmospheric transport patterns from selected nuclear risk sites for the GIS-based studies of vulnerability to radioactive deposition and risk assessment of the nuclear risk sites impact.

The nuclear risk sites of concern (in total 11) selected in this study are nuclear power plants located in Russia (Kola and Leningrad NPPs), Finland (Loviisa and Olkiluoto NPPs), Sweden (Barsebaeck, Oskarshamn, and Ringhals NPPs), Lithuania (Ignalina NPP), groups of the British and German NPPs as well as the Novaya Zemlya test site (Russia). The geographical regions and countries of interest are the North and Central European countries and Northwest Russia.

Once the nuclear risk sites and geographical region of interest were defined, it is of particular interest to answer the following questions: Which geographical territories are at highest risk from the hypothetical accidental releases at selected NRSs? What are probabilities for radionuclide atmospheric transport to different neighboring countries in a case of accidents at these NRSs?

To answer these questions we applied several research tools developed within the Arctic Risk Project (*AR-NARP, 2001-2003*). The first research tool is an isentropic trajectory model to calculate a multiyear (1991-1996) dataset of 5-day forward trajectories that originated over the NRS locations at various altitudes. As input data for modeling purposes we used NCAR meteorological gridded fields. The second research tool is a set of statistical methods (including exploratory, cluster, and probability fields analyses) for analysis of trajectory modeling results.

The results of probabilistic analysis of trajectory modeling results for 11 NRSs are presented as a set of various indicators of the NRS possible impact on geographical regions of interest. In this study, we calculated, constructed, and evaluated several indicators based on trajectory modeling results: 1) atmospheric transport pathways (ATP), 2) airflow (AF) probability fields, 3) fast transport (FT) probability fields, 4) maximum reaching distance (MRD), 5) maximum possible impact zone (MPIZ), 6) precipitation factor (PF) fields, and 7) typical transport time (TTT) fields. To evaluate the temporal variability of all these indicators, an analysis was performed annually, seasonally, and monthly.

The NRS possible impact (on the concrete geographical region, territory, country, site, etc.) **due to atmospheric transport from NRS after hypothetical accidental releases of radioactivity <u>can be properly estimated</u> based on a combined interpretation of the indicators** (simple characteristics, atmospheric transport pathways, airflow and fast transport probability fields, maximum reaching distance and maximum possible impact indicators, typical transport time and precipitation factor fields) **for different time periods** (annual, seasonal, and monthly) **for any selected NRSs** (both separately for each site or grouped for several sites) **in the Euro-Arctic region**. Such estimation could be the useful input information for the decision-making process and planning of emergency response systems at risk sites of nuclear, chemical, biological, etc. danger.

For all selected NRSs the westerly atmospheric transport dominates throughout the year within the boundary layer. For NRSs located closer to the North Atlantic Ocean region (i.e. blocks of the British (BBP) and German (BGP) NPPs, and Barsebaeck NPP (BBP)), the boundaries of the AF

35

probability fields are extended farther (approximately on 1/3 in comparison with other NRSs) in the western direction from the sites. For the block of the British NPPs (BBP), Oskarshamn NPP (ONP), and Olkiluoto NPP (TRS), the airflow pattern is shifted toward the northeast of the site. For the Ignalina NPP (INP), the airflow pattern is shifted toward the southeast of the site.

On an annual scale, among NRSs there are two: one with the highest and one with the lowest MRD areas. For the Novaya Zemlya Test Site (NZS), this area is equal to $903.5 \cdot 10^4$ km^2 with a maximum during winter, and for the Oskarshamn NPP (ONP), it is equal to $595.1 \cdot 10^4$ km^2 with a minimum during spring. Moreover, for NZS, the MPIZ area - $91.5 \cdot 10^4$ km^2 - is the highest among the sites with a minimum in May and a maximum in December.

Considering Denmark as a country of concern it should be noted that throughout the year after the first 12 hours of atmospheric transport: 1) BNP will always represent the highest risk of atmospheric transport to Denmark, especially during spring and fall, and 2) BGP shows the possible impact of 60-80% of AHPPI as well as BBP shows the possible impact of 10-25% of AHPPI over the Danish territory.

It should be noted that the suggested probabilistic indicators of the risk site possible impact could be applicable for initial estimates of probability of atmospheric transport in the event of an accidental release at the risk sites and for improvement in planning the emergency response to radionuclide releases from the risk site locations. And furthermore, they are important input data for the social and economical consequences studies of the risk site impact on population and environment for the neighbouring countries as well as for the multidisciplinary risk and vulnerability analysis, and probabilistic assessment of the meso-, regional-, and long-range transport of radionuclides.

ACKNOWLEDGMENTS

REFERENCES

AR-NARP, **2001-2003**: On-going Project Atmospheric Transport Pathways, Vulnerability and Possible Accidental Consequences from the Nuclear Risk Sites in the European Arctic (*Arctic Risk*) of the NARP: Nordic Arctic Research Programme. WWW-site: http://www.dmi.dk/f+u/luft/arctic-risk/main.html; Leader: Dr. Alexander Baklanov, alb@dmi.dk.

Baklanov A., Mahura A., Jaffe D., Thaning L., Bergman R., Andres R., Merrill J., **1998**: Atmospheric Transport Pathways and Possible Consequences after a Nuclear Accident in North-West Russia. *The 11th World Clear Air and Environment Congress*. S. Africa, Durban. 14-18 September 1998. Volume 2. E6-1: 6 pp.

Baklanov A., Mahura A., Jaffe D., Thaning L., Bergman R., Andres R., **2001**: Atmospheric Transport Patterns and Possible Consequences for the European North after a Nuclear Accident. *Journal of Environment Radioactivity,* Vol. 60, Issue 1-2, pp. 1-26.

Baklanov A., Mahura A., **2001**: Atmospheric Transport Pathways, Vulnerability and Possible Accidental Consequences from Nuclear Risk Studies: Methodology for Probabilistic Atmospheric Studies. *Danish Meteorological Institute Scientific Report,* 01-09, ISBN: 87-7478-450-1, 43 p.

Baklanov A., Sørensen J.H., **2001**: Parameterisation of radionuclide deposition in atmospheric dispersion models. *Phys. Chem. Earth, (B)*, **26**, 787–799.

Baklanov A., Mahura A., Sorensen J.H., Rigina O., **2002a**: Methodology for Risk Analysis based on Atmospheric Dispersion Modelling from Nuclear Risk Sites in Northern Europe. *Danish Meteorological Institute Scientific Report*, 55p., (*in preparation*), Summer-Fall 2002.

Baklanov A., Mahura A., Rigina O., **2002b**: Nuclear Risk and Vulnerability in the Arctic: New Method for Multidisciplinary Assessments. *Extended Abstracts of the Environmental Radioactivity in the Arctic & Antarctic Conference*, S-Petersburg, Russia, 16-20 June 2002, pp. 397-400.

Baklanov A., Mahura A., Rigina O., **2002c**: Nuclear Risk and Vulnerability: Approach for Multidisciplinary Assessments. *Extended Abstracts of the International Conference on Radioactivity in the Environment*, Principality of Monaco, 2-5 September 2002, pp. 87-92.

Bergman R., Agren G., **1999**: Radioecological Characteristcis of Boreal and Sub-Arctic Environments in Northern Sweden: focus on long-term transfer of radioactive deposition over food-chains. *Proceedings of the 4th International Conference on Environmental Radioactivity in the Arctic,* Edinburgh, Scotland, 20-23 Setember 1999, pp. 91-94.

CERUM, **2000**: Nuclear Risk, Environmental, and Development Co-operation in the North of Europe. *Extended Abstracts of the International Conference,* Apatity, Russia, 19-23 June 1999, 239p.

INTAS, **2000**: Assessment of Potential Risk of Environmental Radioactive Contamination in Northern Europe from Terrestrial Muclear Units in North-West Russia. Research Report, *INTAS Project 96-1802, Research Report,* 125p., November 2000.

Jaffe D., Mahura A., Andres R., **1997a**: Atmospheric Transport Pathways to Alaska from Potential Radionuclide Sites in the Former Soviet Union. *Research Report, UAF-ADEC Joint Project 96-001,* 71p.

Jaffe D., Mahura A., Andres R., Baklanov A., Thaning L., Bergman R., Morozov S., **1997b**: Atmospheric Transport from the Kola Nuclear Power Plant. *Research Report, UAF-FOA-BECN Joint Project, BECN,* Tromsø University, Norway, Fall 1997, 61p.

Mahura A., Jaffe D., Andres R., Dasher D., Merrill J., **1997a**: Atmospheric Transport Pathways to Alaska from Potential Radionuclide Sites in the Former Soviet Union. *Proceedings of ANS 6th Topical Meeting on Emergency Preparedness and Response*, San Francisco, California, USA, April 1997, Vol 1, pp. 173-174.

Mahura A., Jaffe D., Andres R., Dasher D., Merrill J., **1997b**: Atmospheric Transport Pathways from the Kola Nuclear Power Plant. *Extended abstracts of Intentional Symposium on Environmental Pollution of the Arctic and The 3rd International Conference on Environmental Radioactivity in the Arctic*, Tromsø, Norway, 1-5 June 1997, Vol 2, pp. 52-54.

Mahura A., Jaffe D., Andres R., **1999a**: Air Flow Patterns and Precipitation Probability Fields for the Kola NPP. *Extended Abstracts of the International Conference "Nuclear Risks, Environmental and Development Cooperation in the North of Europe"*, Apatity, Russia, 19-23 June 1999, pp. 87-93.

Mahura A., Jaffe D., Andres R., Merrill J., **1999b**: Atmospheric transport pathways from the Bilibino nuclear power plant to Alaska. *Atmospheric Environment*, 33/30, pp. 5115-5122.

Mahura A., **2001**: Probabilistic Assessment of Atmospheric Transport Patterns from Nuclear Risk Sites, *Ph.D. Thesis*, 172p.

Mahura A., Andres R., Jaffe D., **2001**: Atmospheric transport patterns from the Kola Nuclear Reactors. *CERUM Northern Studies No. 24*. Umeå University, Sweden, 33p.

Mahura A., **2002**: Assessment of Impact of Russian Nuclear Fleet Operations on Russian Far Eastern Coastal Regions. *IIASA interim report IR-02-004*, January 2002, 76p.

Mahura A., Baklanov A., Sørensen J. H., **2002a**: Methodology for Evaluation of Possible Consequences of Accidental Atmospheric Releases of Hazardous Matter. *Accepted to publication in the Rad Prot Dosim, 8p., ref#2154*.

Mahura A., Baklanov A., Rigina O., Parker F.L., **2002b**: Statistical Analysis of Atmospheric Transport from the Nuclear Risk Sites in the Arctic Region. *Extended Abstracts of the Environmental Radioactivity in the Arctic & Antarctic Conference*, St.Petersburg, Russia, 16-20 June 2002, pp. 119-123.

Mahura A., Baklanov A., **2002c**: Probabilistic Analysis of Atmospheric Transport Patterns from Nuclear Risk Sites in Euro-Arctic Region. *Danish Meteorological Institute Scientific Report*, Fal 2002, 87p.

Mahura A., Baklanov A., Rigina O., **2002d**: Probabilistic Indicators of Atmospheric Transport for Emergency Preparedness. *Submitted for Peer-Review Process to Tellus*, 8p.

Mahura A., Baklanov A., **2002**: Evaluation of Source-Receptor Relationship for Pollutans Using Probability Fields Analysis. *Danish Meteorological Institute Scientific Report*, 67 p., Fal 2002 – Win 2003, (*in preparation*).

Mahura A., Baklanov A., Sorensen J.H., Rigina O., **2003**: Probabilistic Analysis of Atmospheric Radionuclide Dispersion and Deposition Patterns from Nuclear Risk Sites in Euro-Arctic Region. *Danish Meteorological Institute Scientific Report*, Fal 2002, 80p.

Merrill J., Bleck R., Boudra D.B., **1985**: Techniques of Lagrangian Trajectory Analysis in Isentropic Coordinates. *Monthly Weather Review*, Vol 114, pp. 571-581.

Rigina O., Baklanov A., **1999**: Integration of Mathematical Modeling and GIS-analysis for Radiation Risk Assessment. *Extended Abstracts of the International Conference* "*Nuclear Risks, Environmental and Development Cooperation in the North of Europe*", Apatity, Russia, 19-23 June 1999, (manuscript).

Rigina O., **2001**: Integration of Remote Sensing, Mathematical Modeling and GIS for Complex Environmental Impact Assessment in the Kola Peninsula, Russian North. *Ph.D. Thesis*, April 2001, Geographical Institute of Copenhagen University, Copenhagen: IGUK Press.

Rigina O., Baklanov A., **2002**: Regional radiation risk and vulnerability assessment by integration of mathematical modeling and GIS-analysis. *J. Environment International*, Vol 27, No 6, pp. 1-14.

Sass B.H., Nielsen N.W., Jørgensen J.U., Amstrup B., Kmit M., **2000**: The operational HIRLAM system, *DMI Technical report* 00-26, Copenhagen, Denmark. http://www.dmi.dk/f+u/publikation/tekrap/2000/Tr00-26.pdf.

Sørensen J.H., Laursen L., Rasmussen A., **1994**: Use of DMI-HIRLAM for Operational Dispersion Calculations, in: *Air Pollution Modeling and Its Application* X, edited by S.V.Gryning & M.M.Millan, Plenum Press, pp. 373-381.

Sørensen, J.H. **1998**: Sensitivity of the DERMA Long-Range Gaussian Dispersion Model to Meteorological Input and Diffusion Parameters. *Atmos. Environ*, Vol 32, pp. 4195-4206

ÖCB, **2000**: Nuclear Risks, Environmental and Development Cooperation in the North of Europe. *FRN publication,* CERUM, University of Umea, Sweden, 240p.

ABBREVIATIONS

AR-NARP   "Arctic Risk" Project - Nordic Arctic Research Programme
AF   AirFlow
AHHPI   Area of the Highest Probability of the Possible Impact
AMC   Absolute Maximum Cell
ATP   Atmospheric Transport Pathways
BBP   Block of the British NPPs
BGP   Block of the German NPPs
BNP   Barsebaeck Nuclear Power Plant
DERMA   Danish Emergency Response Model for Atmosphere
DMI   Danish Meteorological Institute
ECMWF   European Center for Medium Weather Forecast
FT   Fast Transport
GIS   Geographic Information System
HIRLAM   HIgh Resolution Limited Area Model
INP   Ignalina Nuclear Power Plant
KNP   Kola Nuclear Power Plant
LNP   Leningrad Nuclear Power Plant
LRS   Loviisa Nuclear Power Plant
MPIZ   Maximum Possible Impact Zone
MRD   Maximum Reaching Distance
NCAR   National Center for Atmospheric Research
NCEP   National Center for Environmental Prediction
NPP   Nuclear Power Plant
NRS   Nuclear Risk Site
NZS   Novaya Zemlya Test Site
ONP   Oskarshamn Nuclear Power Plant
PF   Precipitation Factor
RNP   Ringhals Nuclear Power Plant
TRS   Olkiluoto (TVO) Nuclear Power Plant
TTT   Typical Transport Time
UDHR   Unit Discrete Hypothetical Release

APPENDECIES

1. *MONTHLY VARIATIONS OF AIRFLOW PATTERNS FROM NRSs*

2. *MONTHLY VARIATIONS OF FAST TRANSPORT PATTERNS FROM NRSs AFTER 12 HOURS OF ATMOSPHERIC TRANSPORT*

3. *MONTHLY VARIATIONS OF FAST TRANSPORT PATTERNS FROM NRSs AFTER 24 HOURS OF ATMOSPHERIC TRANSPORT*

4. *MONTHLY VARIATIONS OF MAXIMUM POSSIBLE IMPACT ZONE AND MAXIMUM REACHING DISTANCE INDICATORS FOR NRSs*

DANISH METEOROLOGICAL INSTITUTE

Scientific Reports

Scientific reports from the Danish Meteorological Institute cover a variety of geophysical fields, i.e. meteorology (including climatology), oceanography, subjects on air and sea pollution, geomagnetism, solar-terrestrial physics, and physics of the middle and upper atmosphere.

Reports in the series within the last five years:

No. 97-1
E. Friis Christensen og C. Skøtt: Contributions from the International Science Team. The Ørsted Mission - a pre-launch compendium

No. 97-2
Alix Rasmussen, Sissi Kiilsholm, Jens Havskov Sørensen, Ib Steen Mikkelsen: Analysis of tropospheric ozone measurements in Greenland: Contract No. EV5V-CT93-0318 (DG 12 DTEE):
DMI's contribution to CEC Final Report Arctic Trophospheric Ozone Chemistry ARCTOC

No. 97-3
Peter Thejll: A search for effects of external events on terrestrial atmospheric pressure: cosmic rays

No. 97-4
Peter Thejll: A search for effects of external events on terrestrial atmospheric pressure: sector boundary crossings

No. 97-5
Knud Lassen: Twentieth century retreat of sea-ice in the Greenland Sea

No. 98-1
Niels Woetman Nielsen, Bjarne Amstrup, Jess U. Jørgensen: HIRLAM 2.5 parallel tests at DMI: sensitivity to type of schemes for turbulence, moist processes and advection

No. 98-2
Per Høeg, Georg Bergeton Larsen, Hans-Henrik Benzon, Stig Syndergaard, Mette Dahl Mortensen: The GPSOS project Algorithm functional design and analysis of ionosphere, stratosphere and troposphere observations

No. 98-3
Mette Dahl Mortensen, Per Høeg: Satellite atmosphere profiling retrieval in a nonlinear troposphere Previously entitled: Limitations induced by Multipath

No. 98-4
Mette Dahl Mortensen, Per Høeg: Resolution properties in atmospheric profiling with GPS

No. 98-5
R.S. Gill and M. K. Rosengren: Evaluation of the Radarsat imagery for the operational mapping of sea ice around Greenland in 1997

No. 98-6
R.S. Gill, H.H. Valeur, P. Nielsen and K.Q. Hansen: Using ERS SAR images in the operational mapping of sea ice in the Greenland waters: final report for ESA-ESRIN's: pilot projekt no. PP2.PP2.DK2 and 2nd announcement of opportunity for the exploitation of ERS data projekt No. AO2..DK 102

No. 98-7
Per Høeg et al.: GPS Atmosphere profiling methods and error assessments

No. 98-8
H. Svensmark, N. Woetmann Nielsen and A.M. Sempreviva: Large scale soft and hard turbulent states of the atmosphere

No. 98-9
Philippe Lopez, Eigil Kaas and Annette Guldberg: The full particle-in-cell advection scheme in spherical geometry

No. 98-10
H. Svensmark: Influence of cosmic rays on earth's climate

No. 98-11
Peter Thejll and Henrik Svensmark: Notes on the method of normalized multivariate regression

No. 98-12
K. Lassen: Extent of sea ice in the Greenland Sea 1877-1997: an extension of DMI Scientific Report 97-5

No. 98-13
Niels Larsen, Alberto Adriani and Guido DiDonfrancesco: Microphysical analysis of polar stratospheric clouds observed by lidar at McMurdo, Antarctica

No.98-14
Mette Dahl Mortensen: The back-propagation method for inversion of radio occultation data

No. 98-15
Xiang-Yu Huang: Variational analysis using spatial filters

No. 99-1
Henrik Feddersen: Project on prediction of climate variations on seasonel to interannual timescales (PROVOST) EU contract ENVA4-CT95-0109: DMI contribution to the final report:Statistical analysis and post-processing of uncoupled PROVOST simulations

No. 99-2
Wilhelm May: A time-slice experiment with the ECHAM4 A-GCM at high resolution: the experimental design and the assessment of climate change as compared to a greenhouse gas experiment with ECHAM4/OPYC at low resolution

No. 99-3
Niels Larsen et al.: European stratospheric monitoring stations in the Artic II: CEC Environment and Climate Programme Contract ENV4-CT95-0136. DMI Contributions to the project

No. 99-4
Alexander Baklanov: Parameterisation of the deposition processes and radioactive decay: a review and some preliminary results with the DERMA model

No. 99-5
Mette Dahl Mortensen: Non-linear high resolution inversion of radio occultation data

No. 99-6
Stig Syndergaard: Retrieval analysis and methodologies in atmospheric limb sounding using the GNSS radio occultation technique

No. 99-7
Jun She, Jacob Woge Nielsen: Operational wave forecasts over the Baltic and North Sea

No. 99-8
Henrik Feddersen: Monthly temperature forecasts for Denmark - statistical or dynamical?

No. 99-9
P. Thejll, K. Lassen: Solar forcing of the Northern hemisphere air temperature: new data

No. 99-10
Torben Stockflet Jørgensen, Aksel Walløe Hansen: Comment on "Variation of cosmic ray flux and global coverage - a missing link in solar-climate relationships" by Henrik Svensmark and Eigil Friis-Christensen

No. 99-11
Mette Dahl Meincke: Inversion methods for atmospheric profiling with GPS occultations

No. 99-12
Hans-Henrik Benzon; Laust Olsen; Per Høeg: Simulations of current density measurements with a Faraday Current Meter and a magnetometer

No. 00-01
Per Høeg; G. Leppelmeier: ACE - Atmosphere Climate Experiment

No. 00-02
Per Høeg: FACE-IT: Field-Aligned Current Experiment in the Ionosphere and Thermosphere

No. 00-03
Allan Gross: Surface ozone and tropospheric chemistry with applications to regional air quality modeling. PhD thesis

No. 00-04
Henrik Vedel: Conversion of WGS84 geometric heights to NWP model HIRLAM geopotential heights

No. 00-05
Jérôme Chenevez: Advection experiments with DMI-Hirlam-Tracer

No. 00-06
Niels Larsen: Polar stratospheric clouds microphysical and optical models

No. 00-07
Alix Rasmussen: "Uncertainty of meteorological parameters from DMI-HIRLAM"

No. 00-08
A.L. Morozova: Solar activity and Earth's weather. Effect of the forced atmospheric transparency changes on the troposphere temperature profile studied with atmospheric models

No. 00-09
Niels Larsen, Bjørn M. Knudsen, Michael Gauss, Giovanni Pitari: Effects from high-speed civil traffic aircraft emissions on polar stratospheric clouds

No. 00-10
Søren Andersen: Evaluation of SSM/I sea ice algorithms for use in the SAF on ocean and sea ice, July 2000

No. 00-11
Claus Petersen, Niels Woetmann Nielsen: Diagnosis of visibility in DMI-HIRLAM

No. 00-12
Erik Buch: A monograph on the physical oceanography of the Greenland waters

No. 00-13
M. Steffensen: Stability indices as indicators of lightning and thunder

No. 00-14
Bjarne Amstrup, Kristian S. Mogensen, Xiang-Yu Huang: Use of GPS observations in an optimum interpolation based data assimilation system

No. 00-15
Mads Hvid Nielsen: Dynamisk beskrivelse og hydrografisk klassifikation af den jyske kyststrøm

No. 00-16
Kristian S. Mogensen, Jess U. Jørgensen, Bjarne Amstrup, Xiaohua Yang and Xiang-Yu Huang: Towards an operational implementation of HIRLAM 3D-VAR at DMI

No. 00-17
Sattler, Kai; Huang, Xiang-Yu: Structure function characteristics for 2 meter temperature and relative humidity in different horizontal resolutions

No. 00-18
Niels Larsen, Ib Steen Mikkelsen, Bjørn M. Knudsen m.fl.: In-situ analysis of aerosols and gases in the polar stratosphere. A contribution to THESEO. Environment and climate research programme. Contract no. ENV4-CT97-0523. Final report

No. 00-19
Amstrup, Bjarne: EUCOS observing system experiments with the DMI HIRLAM optimum interpolation analysis and forecasting system

No. 01-01
V.O. Papitashvili, L.I. Gromova, V.A. Popov and O. Rasmussen: Northern polar cap magnetic activity index PCN: Effective area, universal time, seasonal, and solar cycle variations

No. 01-02
M.E. Gorbunov: Radioholographic methods for processing radio occultation data in multipath regions

No. 01-03
Niels Woetmann Nielsen; Claus Petersen: Calculation of wind gusts in DMI-HIRLAM

No. 01-04
Vladimir Penenko; Alexander Baklanov: Methods of sensitivity theory and inverse modeling for estimation of source parameter and risk/vulnerability areas

No. 01-05
Sergej Zilitinkevich; Alexander Baklanov; Jutta Rost; Ann-Sofi Smedman, Vasiliy Lykosov and Pierluigi Calanca: Diagnostic and prognostic equations for the depth of the stably stratified Ekman boundary layer

No. 01-06
Bjarne Amstrup: Impact of ATOVS AMSU-A radiance data in the DMI-HIRLAM 3D-Var analysis and forecasting system

No. 01-07
Sergej Zilitinkevich; Alexander Baklanov: Calculation of the height of stable boundary layers in operational models

No. 01-08
Vibeke Huess: Sea level variations in the North Sea – from tide gauges, altimetry and modelling

No. 01-09
Alexander Baklanov and Alexander Mahura: Atmospheric transport pathways, vulnerability and possible accidental consequences from nuclear risk sites: methodology for probabilistic atmospheric studies

No. 02-01
Bent Hansen Sass and Claus Petersen: Short range atmospheric forecasts using a nudging procedure to combine analyses of cloud and precipitation with a numerical forecast model

No. 02-02
Erik Buch: Present oceanographic conditions in Greenland waters

No. 02-03
Bjørn M. Knudsen, Signe B. Andersen and Allan Gross: Contribution of the Danish Meteorological Institute to the final report of SAMMOA. CEC contract EVK2-1999-00315: Spring-to.-autumn measurements and modelling of ozone and active species

No. 02-04
Nicolai Kliem: Numerical ocean and sea ice modelling: the area around Cape Farewell (Ph.D. thesis)

No. 02-05
Niels Woetmann Nielsen: The structure and dynamics of the atmospheric boundary layer

No. 02-06
Arne Skov Jensen, Hans-Henrik Benzon and Martin S. Lohmann: A new high resolution method for processing radio occultation data

No. 02-07
Per Høeg and Gottfried Kirchengast: ACE+: Atmosphere and Climate Explorer

No. 02-08
Rashpal Gill: SAR surface cover classification using distribution matching

No. 02-09
Kai Sattler, Jun She, Bent Hansen Sass, Leif Laursen, Lars Landberg, Morten Nielsen og Henning S. Christensen: Enhanced description of the wind climate in Denmark for determination of wind resources: final report for 1363/00-0020: Supported by the Danish Energy Authority

No. 02-10
Michael E. Gorbunov and Kent B. Lauritsen: Canonical transform methods for radio occultation data

No. 02-11
Kent B. Lauritsen and Martin S. Lohmann: Unfolding of radio occultation multipath behavior using phase models

No. 02-12
Rashpal Gill: SAR image classification using fuzzy screening method

No. 02-13
Kai Sattler: Precipitation hindcasts of historical flood events

No. 02-14
Tina Christensen: Energetic electron precipitation studied by atmospheric x-rays